

Four top final states with NLO accuracy in perturbative QCD: 3 lepton channel

Nikolaos Dimitrakopoulos and Malgorzata Worek

*Institute for Theoretical Particle Physics and Cosmology, RWTH Aachen University,
D-52056 Aachen, Germany*

E-mail: ndimitrak@physik.rwth-aachen.de, worek@physik.rwth-aachen.de

ABSTRACT: We examine the effect of higher-order QCD corrections on the four top-quark production cross section in the 3 lepton decay channel. Top-quark and W gauge-boson decays are included at next-to-leading order in perturbative QCD. The narrow-width approximation, that preserves spin correlations, is used to perform the calculation for this complex $2 \rightarrow 12$ (13) process. We present differential cross-section distributions of top-quark decay products for the LHC Run III energy of $\sqrt{s} = 13.6$ TeV, using realistic selection cuts. Our results show that QCD corrections and jet radiation in top-quark and W decays can lead to significant changes in shapes of basic kinematic distributions and, therefore, need to be included for the accurate description of $pp \rightarrow t\bar{t}\bar{t} + X$ process in the 3ℓ decay channel. The NLO QCD results obtained in this work are important in the context of the recent observation of the $pp \rightarrow t\bar{t}\bar{t} + X$ process by the ATLAS and CMS collaborations and are of great significance for the High-Luminosity phase of the LHC.

KEYWORDS: Higher-Order Perturbative Calculations, Specific QCD Phenomenology, Top Quark

TTK-24-32, P3H-24-062

Contents

1	Introduction	1
2	Description of the calculation	3
3	Computational setup	5
4	Integrated fiducial cross sections	6
5	Differential fiducial cross-section distributions	11
6	Summary and Outlook	21

1 Introduction

The production of four top quarks ($t\bar{t}t\bar{t}$) represents one of the rarest and most intriguing processes studied at the Large Hadron Collider (LHC). As the heaviest known elementary particle, the top quark plays a crucial role in the Standard Model (SM) of particle physics, particularly in the electroweak symmetry-breaking mechanism and the coupling to the Higgs boson. The simultaneous production of four top quarks in high-energy proton-proton collisions offers a unique opportunity to probe the SM at the highest energy scales and to search for potential new physics beyond it. In the SM, the production of four top quarks is predicted to occur with a low cross section [1], making it a challenging process to observe. However, its study is vital for several reasons. Firstly, the production of four top quarks provides a rigorous test of SM predictions, especially in the context of QCD and the complex interaction of top quarks. Measuring the $pp \rightarrow t\bar{t}t\bar{t} + X$ process and comparing it with theoretical predictions allows physicists to validate or refine existing Monte Carlo tools and approximations they employ. Secondly, the large mass of the top quark provides a substantial coupling to the Higgs boson ($Y_t = \sqrt{2} m_t/v \approx 1$), making the top quark a key player in the understanding of the Higgs mechanism. The production of four top quarks is sensitive to the top-Higgs interaction and the Higgs-boson width, offering insight into the nature of electroweak symmetry breaking [2, 3]. Thirdly, many theories beyond the SM, such as supersymmetry, extra dimensions, and models involving new heavy particles, predict an increase in the production rate of the four top quarks [4–15]. For example, some new particles or interactions may lead not only to an increased cross section, but also to new signatures in the four top events that would affect various dimensionful and dimensionless differential cross-section distributions. Any deviation from SM predictions will, of course, signal the presence of new physics beyond the SM (BSM). However, for all of these BSM studies, a good theoretical control of the SM $pp \rightarrow t\bar{t}t\bar{t} + X$ process is an essential condition for the correct interpretation of possible signals of new physics that may appear in this channel. Fourthly, four top-quark production at hadron colliders can also be examined in the Standard Model Effective Field Theory. Although the $pp \rightarrow t\bar{t}$ process seems to be the leading process for exploring new physics in the top-quark sector, there are situations where dimension-six operators are suppressed in this process. In such situations, a much better way to investigate these contributions can be through the direct production of four top quarks [16–19]. Fifthly, the decay

of four top quarks results in various and complex final states with multiple leptons, light- and b -jets as well as missing transverse momentum from escaping neutrinos, providing a rich environment for testing advanced particle reconstruction methods and analysis techniques. These final states also allow for the exploration of rare decay modes and interactions that are otherwise difficult to study. Finally, observing four top-quark production at the LHC is a significant experimental challenge due to the rarity of the process and the complexity of the resulting events. Sophisticated analysis methods, including machine learning algorithms, have to be employed to distinguish signal events from the large background processes. Despite these challenges, the continued study of four top-quark production holds great potential for advancing our understanding of fundamental interactions within the SM and possibly uncovering new phenomena that could reshape our understanding of the universe.

The ATLAS and CMS collaborations at the CERN LHC performed searches for $t\bar{t}t\bar{t}$ production using the pp collision data recorded between 2015 and 2018 at a center-of-mass energy of 13 TeV, covering the decay channels with zero to four leptons. These searches found evidence for $t\bar{t}t\bar{t}$ production with a significance of more than 3 standard deviations from the background-only hypothesis, however, the observation level of 5 standard deviations was not reached [20, 21]. Finally, in 2023 with the help of the updated identification techniques for charged leptons and b -jets, and by employing a revised multivariate analysis strategy to distinguish the signal process from the main backgrounds, the four top-quark production was observed with a significance larger than 5 standard deviations by both the ATLAS and CMS collaborations [22, 23]. In both measurements, events with two same-sign, three, and four charged leptons (electrons and muons) and additional jets have been analysed. Although the observation of the $pp \rightarrow t\bar{t}t\bar{t} + X$ process marked a milestone in the top-quark physics program at the LHC, detailed measurements of $pp \rightarrow t\bar{t}t\bar{t} + X$ in all final states, i.e. in the 4ℓ , 3ℓ , 2ℓ (including two same-sign as well as two opposite-sign charged leptons), 1ℓ and 0ℓ decay channels, along with various differential cross-section distributions of interest to SM and beyond SM physics, are still pending.

As far as theory is concerned, numerous theoretical predictions regarding the $pp \rightarrow t\bar{t}t\bar{t}$ process can be found in the literature. Briefly, they can be divided into two categories, predictions involving the stable top quark, which are important for the overall normalization of the process, and predictions incorporating top-quark decays, which are needed when studying various differential cross-section distributions in various fiducial phase-space regions that are of interest to the ATLAS and CMS collaborations. For the case of stable top quark, the first NLO QCD predictions were calculated in Ref. [1] and later recomputed in Refs. [24, 25]. The so-called complete NLO corrections, that include all leading and subleading contributions together with their corresponding higher-order corrections at perturbative orders from $\mathcal{O}(\alpha_s^5)$ to $\mathcal{O}(\alpha_s^5)$, were provided in Ref. [26], where it was shown in detail that accidental cancellations occurred between different terms in α_s and α for the $pp \rightarrow t\bar{t}t\bar{t} + X$ process. Consequently, the higher-order effects for this process are dominated by α_s corrections to the leading QCD process at $\mathcal{O}(\alpha_s^4)$. Finally, the calculation at the next-to-leading logarithmic accuracy was also performed for the $pp \rightarrow t\bar{t}t\bar{t} + X$ process [27]. To provide theoretical predictions in the fiducial phase-space regions, it is necessary to study the final state with 12 particles, which greatly complicates the calculation of higher-order corrections for this process. Depending on the decay mode considered, the corresponding final state consists of four b -jets, additional light jets, and/or charged leptons together with (significant) missing transverse momentum from neutrinos escaping detection. To model top-quark decays, one can straightforwardly incorporate leading order $t \rightarrow W^+b \rightarrow \ell^+\nu_\ell b$ or $t \rightarrow W^+b \rightarrow q\bar{q}'b$ decays and employ parton shower approximations for additional collinear parton splitting or soft gluon emission contributions. This method has already been utilised in the case of the $pp \rightarrow t\bar{t}t\bar{t} + X$ process in the 1ℓ decay channel [28]. Another approach is to calculate higher-order

QCD corrections not only to the production of four top quarks, but also in top-quark decays already at the level of matrix elements, thereby preserving spin correlations at the NLO level in QCD. For this purpose, in Ref. [29] the narrow-width approximation (NWA) was utilised to obtain higher-order predictions in the 4ℓ decay channel. Unfortunately, results for other decay channels are not yet available in the literature.

The purpose of this article is to remedy this situation and to provide theoretical predictions for the $pp \rightarrow t\bar{t}t\bar{t} + X$ process in the 3ℓ decay channel, which include higher-order QCD corrections to the production and decays of four top quarks. Similarly to the case of the 4ℓ decay channel, the NWA will also be used here. Such calculations would not only include all spin correlations for $2 \rightarrow 12$ processes at the NLO level in QCD, but would also allow us to use arbitrary cuts for the observed final states. In this way, the magnitude of higher-order corrections and the size of the theoretical uncertainties due to scale dependence can be verified in the realistic environment studied by the ATLAS and CMS collaborations.

The article is organized as follows. In Section 2, we briefly describe the calculations we perform. Our computational setup is provided in Section 3. Our LO and NLO QCD integrated (fiducial) cross-section results are discussed in Section 4. On the other hand, various differential cross-section distributions are provided and analysed in Section 5. Section 6 closes the text and discusses some obvious further directions of research.

2 Description of the calculation

The production of four top quarks, while rare, can occur in high-energy pp collisions when the center-of-mass energy of the colliding partons exceeds the $4m_t$ threshold. The unstable top quarks decay further into various final states, including those with 4ℓ , 3ℓ , 2ℓ , 1ℓ or 0ℓ . In this study, our focus lies on the 3ℓ decay channel, where one W^\pm gauge boson decays hadronically while the remaining three W gauge bosons decay leptonically. Therefore, the processes that we consider are as follows:

$$\begin{aligned} pp \rightarrow t\bar{t}t\bar{t} + X &\rightarrow W^+W^-W^+W^-b\bar{b}b\bar{b} + X \rightarrow \ell^+\nu_\ell\ell^-\bar{\nu}_\ell\ell^+\nu_\ell q\bar{q}'b\bar{b}b\bar{b} + X, \\ pp \rightarrow t\bar{t}t\bar{t} + X &\rightarrow W^+W^-W^+W^-b\bar{b}b\bar{b} + X \rightarrow \ell^+\nu_\ell\ell^-\bar{\nu}_\ell\ell^-\bar{\nu}_\ell q\bar{q}'b\bar{b}b\bar{b} + X, \end{aligned} \quad (2.1)$$

where $\ell^\pm = e^\pm, \mu^\pm$ as well as $q\bar{q}' = d\bar{u}, s\bar{c}$ or $q\bar{q}' = u\bar{d}, c\bar{s}$ for W^- and W^+ respectively. At LO we only consider contributions of the order of $\mathcal{O}(\alpha_s^4\alpha^8)$ as these are the dominant ones, see e.g. Ref. [26]. In this case, the production of four top quarks occurs exclusively through QCD interactions and the electroweak couplings become relevant only during the decay phase. In addition, we calculate NLO QCD corrections of the order of $\mathcal{O}(\alpha_s^5\alpha^8)$ to the aforementioned Born contributions. The unstable top quarks and W bosons are treated in the NWA that allows us to separate the production and the decay stages of the four top quarks. In this approximation, by taking the limits $\Gamma_t/m_t, \Gamma_W/m_W \rightarrow 0$ we force the intermediate resonances to be on-shell. This means that only diagrams with four intermediate top-quark resonances are considered in the calculation. Off-shell effects related to triple, double, single and non-resonant top-quark contributions as well as finite top-quark and W width effects are simply neglected throughout the calculation. The neglected contributions are suppressed by the Γ/m ratio for sufficiently inclusive observables [30]. They can, however, be enhanced in specific phase-space regions, like for example in the high p_T tail of various dimensionful observables or in the vicinity of kinematical thresholds/edges, see e.g. Refs. [31–35]. There is no doubt that the full off-shell prediction should be used if available, as it provides the most realistic description of the studied processes. However, obtaining NLO QCD results with full off-shell effects for the $2 \rightarrow 12$ process, especially when hadronic

decays of the W^\pm gauge boson are involved, is not only computationally demanding but also very cumbersome, see Ref. [36] for the simpler case of $t\bar{t}$ production. Consequently, for the $pp \rightarrow t\bar{t}\bar{t} + X$ process in the 3ℓ decay channel, we focus on the on-shell approximation only. On the other hand, the separation of production and decays inherited in the NWA allows us to analyze the importance of higher-order effects at these two stages separately. Indeed, we can examine scenarios in which QCD corrections are applied both at the production and the decay stages, labelled as NLO_{full} , as well as scenarios in which QCD corrections are solely applied during the production stage, denoted as $\text{NLO}_{\text{LO}_{\text{dec}}}$. In this case, top-quark decays are considered with the LO accuracy only. In addition, we can assess the impact of expanding the top-quark width in the calculation, referred to as NLO_{exp} . All the aforementioned approaches have been introduced in Ref. [29].

At LO, two types of subprocesses contribute to the processes listed in Eq. (2.1), namely gg and $q\bar{q}/\bar{q}q$, where $q = u, d, c, s, b$. The former contribution is the dominant one with 72 Feynman diagrams, while the latter consists of 14 Feynman diagrams only and accounts for almost 12% of the LO (fiducial) cross section. At NLO, we compute both virtual and real emission contributions. The virtual corrections are obtained by taking the interference of the sum of all one-loop diagrams with the Born amplitudes. For the real emission part, we can have an additional parton in the final state, thus, the following subprocesses contribute: $gg, q\bar{q}/\bar{q}q, qg/gq, \bar{q}g/g\bar{q}$, where $q = u, d, c, s, b$. For the $gg, q\bar{q}/\bar{q}q$ initiated subprocesses the extra parton is always a gluon, that can be emitted during both the production and decay stages. For the $qg/gq, \bar{q}g/g\bar{q}$ subprocesses the extra light- or b -quark is emitted only at the production stage of the process. Our NLO calculations are performed within the HELAC-NLO framework [37] that consists of HELAC-1LOOP [38] and HELAC-DIPOLES [39]. The HELAC-1LOOP Monte Carlo library comprises CUTTOOLS [40] for the numerical evaluation of one-loop amplitudes using the OPP reduction method [41–43], and ONELOOP [44] for the evaluation of the scalar integrals. The real emission part is computed within the HELAC-DIPOLES framework, where both the Catani-Seymour [45, 46] and Nagy-Soper [47] subtraction schemes have been implemented for the extraction of soft and collinear singularities. The advantage of the latter approach lies in the fact that in each case, there are fewer terms to be evaluated compared to the Catani-Seymour approach. The difference corresponds to the total number of possible spectators in the process under scrutiny, which are relevant only in the Catani-Seymour case. For this reason, the Nagy-Soper subtraction scheme is our default method throughout the computations. Finally, the phase-space integration is performed and optimised with PARNI [48] and KALEU [49].

Similar to our previous NLO QCD calculations for the $pp \rightarrow t\bar{t}\bar{t}$ process in the 4ℓ decay channel, also in this case we have conducted several cross-checks to ensure the correctness and reliability of our theoretical results. To begin with, we have used two different subtraction schemes for extracting the soft and collinear infrared singularities in the real emission part of the NLO calculation. We have reproduced our NLO QCD results with the help of the Catani-Seymour subtraction scheme and found excellent agreement with the results obtained using the default method. In the case of both subtraction schemes we have also verified the independence of our (complete) real emission results on an additional phase-space restriction imposed by the unphysical parameter α_{max} , see e.g. Refs. [50–53] for the definition of this parameter. Additionally, the cancellation of the infrared $1/\epsilon$ and $1/\epsilon^2$ poles between virtual and real corrections, as provided by the \mathcal{I} -operator, has been checked numerically for several phase-space points for both the gg and $q\bar{q}$ subprocesses. We also monitor the numerical stability by checking Ward identities at every phase-space point. The events which do not pass this check have not been discarded from the calculation of the finite part, but rather recalculated with quadruple precision. On the other hand, for the $q\bar{q}$ subprocess we use the so-called scale test [54], which is

based on momentum rescaling. To further confirm the correctness of our results, we have performed various cross-checks using the MADGRAPH-AMC@NLO [24] and RECOLA [55] Monte Carlo programs. Specifically, with the help of the MADGRAPH-AMC@NLO program we have cross-checked the $1/\epsilon$ and $1/\epsilon^2$ poles, separately for the production and decays of the four top quarks. In the latter case, we explicitly calculated the infrared ϵ poles for $t \rightarrow W^+b \rightarrow q\bar{q}'b$ and $t \rightarrow W^+b \rightarrow l^+\bar{\nu}_l b$. On the other hand, using the RECOLA program we have calculated the aforementioned poles for the whole process, i.e. for the production and decays simultaneously. Finally, the finite part of the 1-loop amplitude has also been cross-checked with RECOLA for a few phase-space points for both gg and $q\bar{q}$ subprocesses.

All our LO and NLO results are stored in modified LES HOUCHE FILES [56] and then converted into ROOT NTUPLE FILES [57, 58]. This allows us to efficiently change renormalisation and factorisation scale settings, use different PDF sets, fairly quickly estimate the internal PDF uncertainties from PDF error sets, produce various (infrared-safe) differential cross-section distributions as well as change their binning or apply more stringent cuts, all without rerunning the entire process from scratch. All these tasks are carried out with the help of the HEPLLOT program [59].

3 Computational setup

We consider the $pp \rightarrow t\bar{t}\bar{t} + X$ process in the 3ℓ decay channel as defined in Eq. (2.1). We provide results at LO and NLO in QCD for the LHC Run III using a center-of-mass-energy of $\sqrt{s} = 13.6$ TeV. Since at the LHC the τ leptons are often analysed separately due to their short lifetime and complex decay pattern, we will not consider them in our analysis. We work in the five-flavor scheme and keep the Cabibbo-Kobayashi-Maskawa mixing matrix diagonal. The numerical values of the SM input parameters that enter our calculations are as follows:

$$\begin{aligned} G_\mu &= 1.1663787 \cdot 10^{-5} \text{ GeV}^{-2}, & m_t &= 172.5 \text{ GeV}, \\ m_W &= 80.379 \text{ GeV}, & \Gamma_W^{\text{NLO}} &= 2.0972 \text{ GeV}, \\ m_Z &= 91.1876 \text{ GeV}, & m_b &= 0 \text{ GeV}. \end{aligned} \quad (3.1)$$

Given that three of the four W bosons decay leptonically and do not receive QCD corrections, we account for higher-order effects in their decays by employing the NLO QCD value for Γ_W , evaluated for $\mu_R = m_W$, in both LO and NLO calculations. The electromagnetic coupling α is evaluated in the G_μ -scheme and it is derived via the following relationship

$$\alpha_{G_\mu} = \frac{\sqrt{2}}{\pi} G_F m_W^2 \left(1 - \frac{m_W^2}{m_Z^2} \right). \quad (3.2)$$

We use the LO (NLO) top-quark width for our LO (NLO) calculations. They are obtained using the formulas in Ref. [60], where $\alpha_s(\mu_R = m_t)$. The values for Γ_t^{LO} and Γ_t^{NLO} read

$$\Gamma_t^{\text{LO}} = 1.4806842 \text{ GeV}, \quad \Gamma_t^{\text{NLO}} = 1.3535983 \text{ GeV}. \quad (3.3)$$

For the LO and NLO QCD results we follow the PDF4LHC working group's recommendation for SM processes [61] and employ the following three PDF sets: MSHT20 [62], NNPDF3.1 [63] and CT18 [64]. We consider the MSHT20 PDF sets as our default sets. Since CT18 lacks a LO PDF set, we replace it with CT14. Specifically, we use the CT14llo PDF set with $\alpha_s(m_Z) = 0.130$ [65] for our LO calculations. The running of the strong coupling is provided with two-loop (one-loop) accuracy at NLO (LO) via

the LHAPDF library [66] where we assume $N_f = 5$. We compute the cross section for two different choices of the renormalization (μ_R) and factorization scale (μ_F)

$$\begin{aligned}\mu_R = \mu_F = \mu_0 &= 2m_t, \\ \mu_R = \mu_F = \mu_0 &= \frac{1}{4}E_T,\end{aligned}\tag{3.4}$$

with E_T given by

$$E_T = \sqrt{m_t^2 + p_T^2(t_1)} + \sqrt{m_t^2 + p_T^2(t_2)} + \sqrt{m_t^2 + p_T^2(\bar{t}_1)} + \sqrt{m_t^2 + p_T^2(\bar{t}_2)},\tag{3.5}$$

where m_t is the nominal mass of the top quark. Finally, top and anti-top momenta needed in the definition of E_T are reconstructed from their decay products. We estimate the uncertainty from missing higher orders by performing a conventional 7-point scale variation around the central $\mu_{R,F}$ values by factors of 2 subject to the constraint $0.5 \leq \mu_R/\mu_F \leq 2$. In addition, we calculate the internal PDF errors for the three PDF sets, using prescriptions provided by each collaboration.

Light- and b -jets are constructed from all partons with $|\eta| < 5$ using the infrared-safe anti- k_T jet algorithm [67] with the resolution parameter $R = 0.4$. All final states have to fulfil the following selection criteria that closely mimic the ATLAS and CMS detector response [22, 23]:

$$\begin{aligned}p_{T,\ell} &> 25 \text{ GeV}, & |y_\ell| &< 2.5, & \Delta R_{\ell\ell} &> 0.4, \\ p_{T,b} &> 25 \text{ GeV}, & |y_b| &< 2.5, & \Delta R_{bb} &> 0.4, \\ p_{T,j} &> 25 \text{ GeV}, & |y_j| &< 2.5, & \Delta R_{bj} &> 0.4.\end{aligned}\tag{3.6}$$

We require exactly 3 charged leptons, at least two light jets and at least 4 b -jets in the final state. Furthermore, we require that at least one pair of light jets (jj) with $\Delta R_{jj} > 0.4$ has an invariant mass (M_{jj}) in the following range

$$|M_{jj} - m_W| < Q_{cut},\tag{3.7}$$

where m_W is the nominal mass of the W gauge boson. Our default setup utilizes $Q_{cut} = 25$ GeV but we also investigate the effect of varying the value of Q_{cut} on the integrated and differential (fiducial) cross sections. The rationale behind the restriction given in Eq. (3.7) is that we want to suppress NLO configurations in which one of the light quarks from the W^\pm decays undergoes recombination with another light or bottom quark. In such cases, the additional jet, if resolved and passed all the cuts, can play the role of a second decay product of the W gauge boson. It is already known that the absence of such a requirement in processes involving hadronic W boson decays can lead to very large $\mathcal{K} = \sigma^{\text{NLO}}/\sigma^{\text{LO}}$ factors, see e.g. Refs. [36, 68, 69]. This is because the topologies described above do not mimic corrections to the born-level amplitude in which the 2 light jets from the W^\pm decays are always well-separated with an invariant mass equal to the W mass. Finally, no restrictions are applied to the kinematics of the additional light- or b -jet (if resolved), as well as the total missing transverse momentum from the three neutrinos.

4 Integrated fiducial cross sections

We start with the LO and NLO integrated fiducial cross-section results for the $pp \rightarrow t\bar{t}\bar{t} + X$ process in the 3ℓ decay channel at the LHC Run III with $\sqrt{s} = 13.6$ TeV. Our default setup utilizes the MSHT20 PDF set as well as the expanded NWA version already described in detail in Ref. [29]. In

PDF	σ^{LO} [ab]	δ_{scale}	σ^{NLO} [ab]	δ_{scale}	δ_{PDF}	$\mathcal{K} = \sigma^{\text{NLO}}/\sigma^{\text{LO}}$
$\mu_R = \mu_F = \mu_0 = 2m_t$						
MSHT20	35.575(2)	+25.883 (73%) -13.982 (39%)	42.25(2)	+8.27 (20%) -9.72 (23%)	+1.76 (4%) -1.32 (3%)	1.19
NNPDF3.1	30.581(2)	+21.781 (71%) -11.853 (39%)	41.89(2)	+8.28 (20%) -9.71 (23%)	+0.89 (2%) -0.89 (2%)	1.37
CT18	37.675(3)	+26.858 (71%) -14.655 (39%)	41.89(2)	+8.20 (20%) -9.62 (23%)	+2.42 (6%) -2.00 (5%)	1.11
$\mu_R = \mu_F = \mu_0 = E_T/4$						
MSHT20	39.424(3)	+29.111 (74%) -15.632 (40%)	44.91(2)	+7.91 (18%) -10.16 (23%)	+1.84 (4%) -1.38 (3%)	1.14
NNPDF3.1	34.193(3)	+24.868 (73%) -13.413 (39%)	44.60(2)	+7.87 (18%) -10.16 (23%)	+0.94 (2%) -0.94 (2%)	1.30
CT18	41.306(3)	+29.728 (72%) -16.169 (39%)	44.50(2)	+7.86 (18%) -10.06 (23%)	+2.51 (6%) -2.08 (5%)	1.08

Table 1: Integrated fiducial cross-section results at LO and NLO in QCD for the $pp \rightarrow t\bar{t}\bar{t} + X$ process in the 3ℓ decay channel at the LHC with $\sqrt{s} = 13.6$ TeV. At NLO QCD, at least one light jet pair that fulfils the criterion of Eq. (3.7) with $Q_{\text{cut}} = 25$ GeV is also required. Results are presented for the (N)LO MSHT20, NNPDF3.1 and CT18 PDF sets. They are evaluated using $\mu_0 = 2m_t$ and $\mu_0 = E_T/4$. The theoretical uncertainties due to 7-point scale variation and internal PDF errors are also given. In the last column, the \mathcal{K} -factor is shown.

this approach, the decay width of the top quark is treated as a perturbative parameter everywhere in the calculation. Thus, a proper expansion in the strong coupling is employed. We will henceforth refer to this approach as $\sigma_{\text{exp}}^{\text{NLO}}$ or simply σ^{NLO} . In Table 1 the LO and NLO results with $|M_{jj} - m_W| < 25$ GeV are given. Our (N)LO cross sections are provided for (N)LO MSHT20, NNPDF3.1 and CT18 PDF sets and two different scale settings, along with their scale and PDF uncertainties. In the last column, the corresponding \mathcal{K} factors are depicted. We can clearly see that the LO results provide only a rough estimate of the cross section due to the large scale uncertainties that are of the order of 70% for both scale choices. However, the situation improves considerably at the NLO level, where these uncertainties decrease to about 20% for both scale settings. In addition, the NLO cross sections obtained with $\mu_0 = 2m_t$ and $\mu_0 = E_T/4$ differ by about 6%, which is well within their corresponding theoretical uncertainties. We can also observe that although at LO the central values for the cross section vary significantly for the three PDF sets, there is a high level of agreement among the results at NLO in QCD. The PDF uncertainties are independent of the scale setting and are of the order of 4% for MSHT20, 6% for CT18 while for NNPDF3.1 they account for only 2%. Finally, the \mathcal{K} -factors are slightly smaller when the dynamical scale setting is employed. However, the size of the \mathcal{K} -factors highly depends on the PDF set under consideration. Consequently, higher-order QCD effects are in the range of 8% – 37%. This large range, discussed in detail in our previous work on the 4ℓ decay channel, is primarily due to the substantial differences in LO cross sections.

In the next step, we examine the dependence of the results on the Q_{cut} cut applied to the two

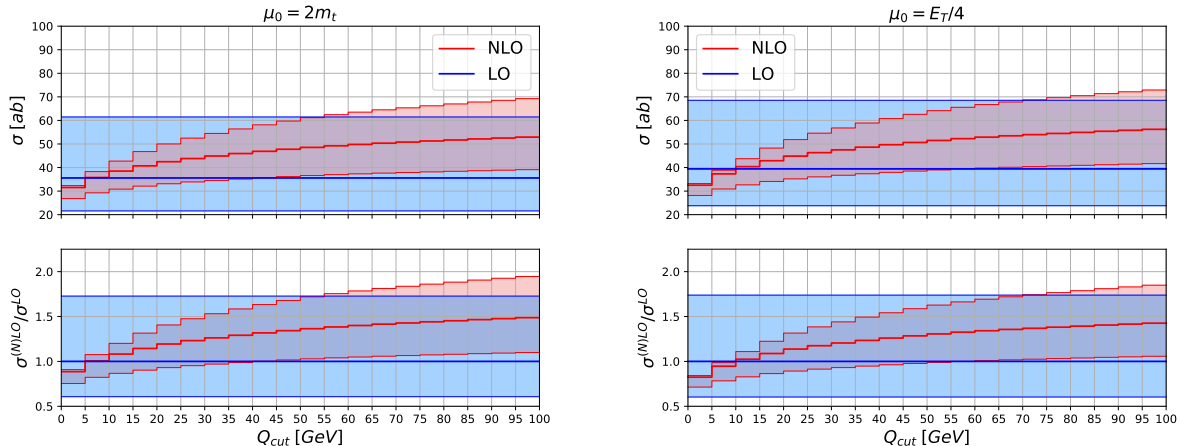


Figure 1: Integrated fiducial cross-section results at LO and NLO in QCD for the $pp \rightarrow t\bar{t}\bar{t} + X$ process in the 3ℓ decay channel at the LHC with $\sqrt{s} = 13.6$ TeV, as a function of Q_{cut} defined as $|M_{jj} - m_W| < Q_{cut}$. Results are shown for the (N)LO MSHT20 PDF set with $\mu_0 = 2m_t$ and $\mu_0 = E_T/4$. The theoretical uncertainties due to 7-point scale variation are also given. The lower panel displays the \mathcal{K} -factor with its uncertainty band along with the relative scale uncertainties of the LO cross section.

light jets in the final state

$$|M_{jj} - m_W| < Q_{cut}. \quad (4.1)$$

As mentioned in Section 3, we expect a high sensitivity of the \mathcal{K} -factor to the choice of Q_{cut} , indicating the need for a closer examination of this issue. This dependence is illustrated in Figure 1. The top panels display the integrated (fiducial) cross section as a function of Q_{cut} at LO and NLO QCD for $\mu_R = \mu_F = \mu_0 = 2m_t$ and $\mu_R = \mu_F = \mu_0 = E_T/4$. The lower panels display the \mathcal{K} -factors together with their uncertainty bands and the relative scale uncertainties of the LO cross sections. As expected, the LO cross section is independent of the Q_{cut} parameter, since the two light jets always come from the decay of the W boson. At NLO, the integrated fiducial cross section increases drastically when the value of Q_{cut} rises, leading to large \mathcal{K} factors close to 1.5 when $Q_{cut} = 100$ GeV. This behavior can be explained by kinematic configurations in which one parton from the W decays is recombined with another parton to form a jet, such that the total number of light-jets coming from the W decays decreases. Although such configurations are not present at LO, they can manifest themselves at NLO. In this case, an additional light jet, originating from another decay or the production stage of the process, which successfully passes all selection criteria, can mimic the second decay product of the W gauge boson. Despite the fact that such configurations can not be directly interpreted as real corrections to the born-level amplitude for the $pp \rightarrow t\bar{t}\bar{t} + X$ process in the 3ℓ decay channel, they have to be taken into account because they contain two light jets in the final state. Exactly these configurations, which can be described as a background process, cause a significant increase in the \mathcal{K} factors. Furthermore, for large values of Q_{cut} , NLO scale uncertainties become similar in size to LO scale uncertainties, emphasizing the fact that such topologies are mainly governed by LO dynamics.

Another interesting feature worth investigating is how our NLO results change if we consider QCD corrections only at the production stage, while treating top quark decays with LO accuracy. We will denote this approach as $\sigma_{LO_{dec}}^{NLO}$. In addition, we would like to investigate the case where the width of the top quark is treated as a fixed parameter in the NLO calculation. We will denote such an approach as σ_{full}^{NLO} . Both approaches were described in detail in Ref. [29]. Since our results are very sensitive

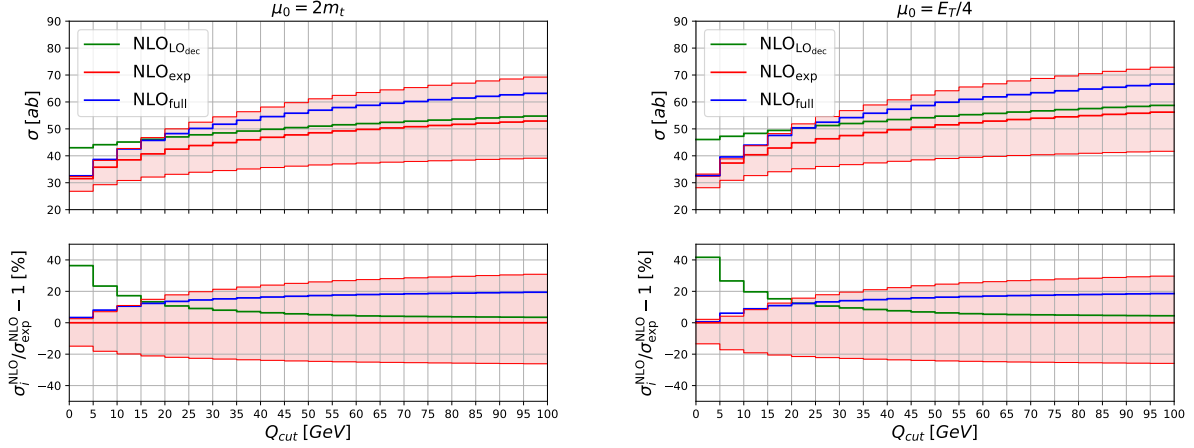


Figure 2: Integrated fiducial cross section for three different scenarios, σ_{exp}^{NLO} , $\sigma_{LO_dec}^{NLO}$ and σ_{full}^{NLO} at NLO in QCD for the $pp \rightarrow t\bar{t}\bar{t} + X$ process in the $3l$ decay channel at the LHC with $\sqrt{s} = 13.6$ TeV, as a function of Q_{cut} defined as $|M_{jj} - m_W| < Q_{cut}$. Results are shown for the NLO MSHT20 PDF set with $\mu_0 = 2m_t$ and $\mu_0 = E_T/4$. The upper plots show absolute predictions while the lower ones illustrate the percentage differences compared to the σ_{exp}^{NLO} case. In all panels, uncertainty bands for the σ_{exp}^{NLO} case are also provided.

to the Q_{cut} cut, we first plot the Q_{cut} dependence of the σ_{exp}^{NLO} , $\sigma_{LO_dec}^{NLO}$ and σ_{full}^{NLO} cross sections for $\mu_0 = 2m_t$ and $\mu_0 = E_T/4$. These results are presented in Figure 2, where the upper panels show the absolute predictions, while the lower panels depict the percentage differences of the various scenarios compared to our default σ_{exp}^{NLO} case. In all panels, the scale uncertainties for the expanded NWA case are also displayed. The increase in the cross sections for high values of Q_{cut} is mainly due to the extra radiation emitted at the production stage. This is evident, as the result for $\sigma_{LO_dec}^{NLO}$ goes closer to the corresponding result for σ_{exp}^{NLO} in this region, indicating that QCD corrections at the production stage are dominant there. Indeed, for Q_{cut} close to 100 GeV, the differences between the two approaches are less than 5%. Conversely, with more stringent cuts applied to the invariant mass of the two light jets, the two approaches can exhibit large differences. For example, when $Q_{cut} = 5$ GeV these differences are of the order of 40%, independently of the scale setting. In addition, for small values of the Q_{cut} cut, the $\sigma_{LO_dec}^{NLO}$ predictions lie completely outside of the uncertainty bands for the expanded case. This is because the invariant mass of the light jets is significantly affected when QCD corrections are applied at the decay stage, particularly when additional radiation is emitted from one of the quarks originating from the W^\pm decays. This leads to a broad distribution in the M_{jj} observable for the σ_{exp}^{NLO} case. In contrast, when QCD corrections are only applied at the production stage, the M_{jj} observable exhibits a sharper peak around the W boson mass. As a consequence, choosing a smaller value for the parameter Q_{cut} removes substantial contributions in the σ_{exp}^{NLO} case, while the $\sigma_{LO_dec}^{NLO}$ case is less affected by this choice. In addition, for values above $Q_{cut} = (20 - 25)$ GeV the σ_{full}^{NLO} result is larger by 15% – 20% compared to the σ_{exp}^{NLO} one for both scale choices. The corresponding differences below $(20 - 25)$ GeV are smaller and almost vanish when the two light jets have an invariant mass very close to the nominal value of the mass of the W gauge boson. We can also see that choosing $Q_{cut} = 25$ GeV as the default value to perform our calculations seems to be a very reasonable choice, as it helps mitigate both the substantial increase in NLO QCD cross-section values, which would lead to significant \mathcal{K} -factors, and the large differences between the various NWA approaches.

Decay treatment	σ_i^{NLO} [ab]	$+\delta_{scale}$ [ab]	$-\delta_{scale}$ [ab]	$\sigma_i^{\text{NLO}}/\sigma_{\text{exp}}^{\text{NLO}} - 1$
$Q_{cut} = 25 \text{ GeV}$				
$\mu_R = \mu_F = \mu_0 = 2m_t$				
full	47.92(2)	+4.56 (10%)	-9.22 (19%)	+13.4%
LO _{dec}	46.76(2)	+12.33 (26%)	-11.51 (25%)	+10.7%
exp	42.25(2)	+8.27 (20%)	-9.72 (23%)	-
$\mu_R = \mu_F = \mu_0 = E_T/4$				
full	50.45(3)	+3.47 (7%)	-9.32 (19%)	+12.3%
LO _{dec}	50.17(3)	+12.95 (26%)	-12.34 (25%)	+11.7%
exp	44.91(2)	+7.91 (18%)	-10.16 (23%)	-
$Q_{cut} \rightarrow \infty$				
$\mu_R = \mu_F = \mu_0 = 2m_t$				
full	82.45(7)	+33.16 (40%)	-24.17 (29%)	+24.2%
LO _{dec}	67.80(3)	+30.49 (45%)	-20.64 (30%)	+2.2%
exp	66.36(5)	+29.01 (44%)	-20.17 (30%)	-
$\mu_R = \mu_F = \mu_0 = E_T/4$				
full	86.7(1)	+33.1 (38%)	-25.0 (29%)	+23.5%
LO _{dec}	72.05(3)	+31.83 (44%)	-21.83 (30%)	+2.6%
exp	70.19(7)	+29.69 (42%)	-21.12 (30%)	-

Table 2: Integrated fiducial cross sections at NLO in QCD for the $pp \rightarrow t\bar{t}\bar{t} + X$ process in the 3ℓ decay channel at the LHC with $\sqrt{s} = 13.6 \text{ TeV}$ for three different scenarios: $\sigma_{\text{full}}^{\text{NLO}}$, $\sigma_{\text{LO}_{\text{dec}}}^{\text{NLO}}$ and $\sigma_{\text{exp}}^{\text{NLO}}$. The results are given with and without the criterion of Eq. (3.7). In the former case, $Q_{cut} = 25 \text{ GeV}$ is required, while in the $Q_{cut} \rightarrow \infty$ scenario there is no restriction on M_{jj} . All results are provided with the NLO MSHT20 PDF set and for $\mu_0 = 2m_t$ and $\mu_0 = E_T/4$. Also given are theoretical uncertainties coming from the scale variation. In the last column the percentage difference to the $\sigma_{\text{exp}}^{\text{NLO}}$ result is also shown.

To conclude this section, in Table 2 we present the integrated fiducial cross-section results along with their scale uncertainties for the various NWA treatments both for our default setup that utilizes

$|M_{jj} - m_W| < Q_{cut} = 25$ GeV and for the case where no restriction on the invariant mass of the two light jets is imposed. This extreme scenario is equivalent to putting $Q_{cut} \rightarrow \infty$ in Eq. (3.7). By comparing the two cases mentioned above, we will be able to directly assess the impact of the Q_{cut} cut in our results. In both cases, results are provided for $\mu_0 = 2m_t$ and $\mu_0 = E_T/4$. Starting our discussion with $Q_{cut} = 25$ GeV, we notice that neglecting higher-order corrections in the top-quark decays overestimates the cross section by about 11% – 12% depending on the scale choice. The difference between σ_{full}^{NLO} and σ_{exp}^{NLO} is of similar magnitude and is at the level of 12% – 13%. These effects are within the corresponding theoretical uncertainties, that are of the order of 23%, 26% and 19% for σ_{exp}^{NLO} , σ_{LOdec}^{NLO} and σ_{full}^{NLO} , respectively. Shifting our focus to the $Q_{cut} \rightarrow \infty$ scenario, we observe larger deviations between σ_{full}^{NLO} and σ_{exp}^{NLO} as compared to the $Q_{cut} = 25$ GeV case. These differences may now be as high as 24%, but are still within the corresponding scale uncertainties. Neglecting higher-order effects in the top-quark decays has less impact when $Q_{cut} \rightarrow \infty$. Indeed, the differences between σ_{LOdec}^{NLO} and σ_{exp}^{NLO} are at the 2% – 3% level only. Most importantly, without any restriction on the invariant mass of the two light jets, the magnitude of the scale uncertainties is substantial for all NWA treatments, reaching values up to 38% – 40% even for the σ_{full}^{NLO} case. The corresponding scale uncertainties for σ_{LOdec}^{NLO} and σ_{exp}^{NLO} are in the range of 42% – 45%, depending on the scale choice. Such sizes of theoretical errors are usually present for LO predictions. Finally, we would like to underline the fact, that in the $Q_{cut} \rightarrow \infty$ case the \mathcal{K} -factors increase significantly. Indeed, for the \mathcal{K} -factors defined according to $\mathcal{K} = \sigma_{exp}^{NLO}/\sigma^{LO}$ we obtain $\mathcal{K} = (1.8 - 1.9)$, whereas for $\mathcal{K} = \sigma_{full}^{NLO}/\sigma^{LO}$, the corresponding values are even up to $\mathcal{K} = (2.2 - 2.3)$. Thus, for the $Q_{cut} \rightarrow \infty$ case not only theoretical uncertainties are substantial, up to even 45%, but also higher-order effects are of the order of 80% – 130%. This emphasises the importance of employing the Q_{cut} cut to restore perturbative convergence in the calculation of higher-order corrections for the $pp \rightarrow t\bar{t}\bar{t} + X$ process in the 3ℓ decay channel.

5 Differential fiducial cross-section distributions

We turn our attention to the differential cross-section distributions. In order to get a full picture of the impact of NLO QCD corrections on different phase-space regions, not just those sensitive to the threshold for $t\bar{t}\bar{t}$ production, it is crucial to analyze various dimensionful and dimensionless observables. All results presented in this section are obtained with the default (N)LO MSHT20 PDF set for the (N)LO calculations. Nevertheless, as in the case of the $pp \rightarrow t\bar{t}\bar{t} + X$ process in the 4ℓ decay channel, also for the 3ℓ decay channel we have examined the stability of our predictions with respect to changing PDF sets. Using the NLO MSHT20, CT18 and NNPDF3.1 PDF sets for the numerous observables, we could conclude that any observed differences are within the estimated theoretical uncertainties due to scale variation. We could also note that the intrinsic PDF uncertainties are more significant in the tails of some dimensionful observables, reaching half the size of the theoretical error due to scale variation. Therefore, also at the differential cross-section level the PDF uncertainties should be carefully considered in the final estimate of the total theoretical error. Returning to the default setup, we begin our discussion by presenting the results at both the LO and NLO levels for $\mu_0 = 2m_t$ and $\mu_0 = E_T/4$ using the $|M_{jj} - m_W| < Q_{cut} = 25$ GeV cut. Our goal is to assess the level of agreement between the two scale settings at different perturbative orders as well as to determine the size of NLO theoretical uncertainties associated with these scale settings.

In Figure 3 we show the sum of the transverse momenta of the four hardest b -jets, $H_{T,b}$, and the

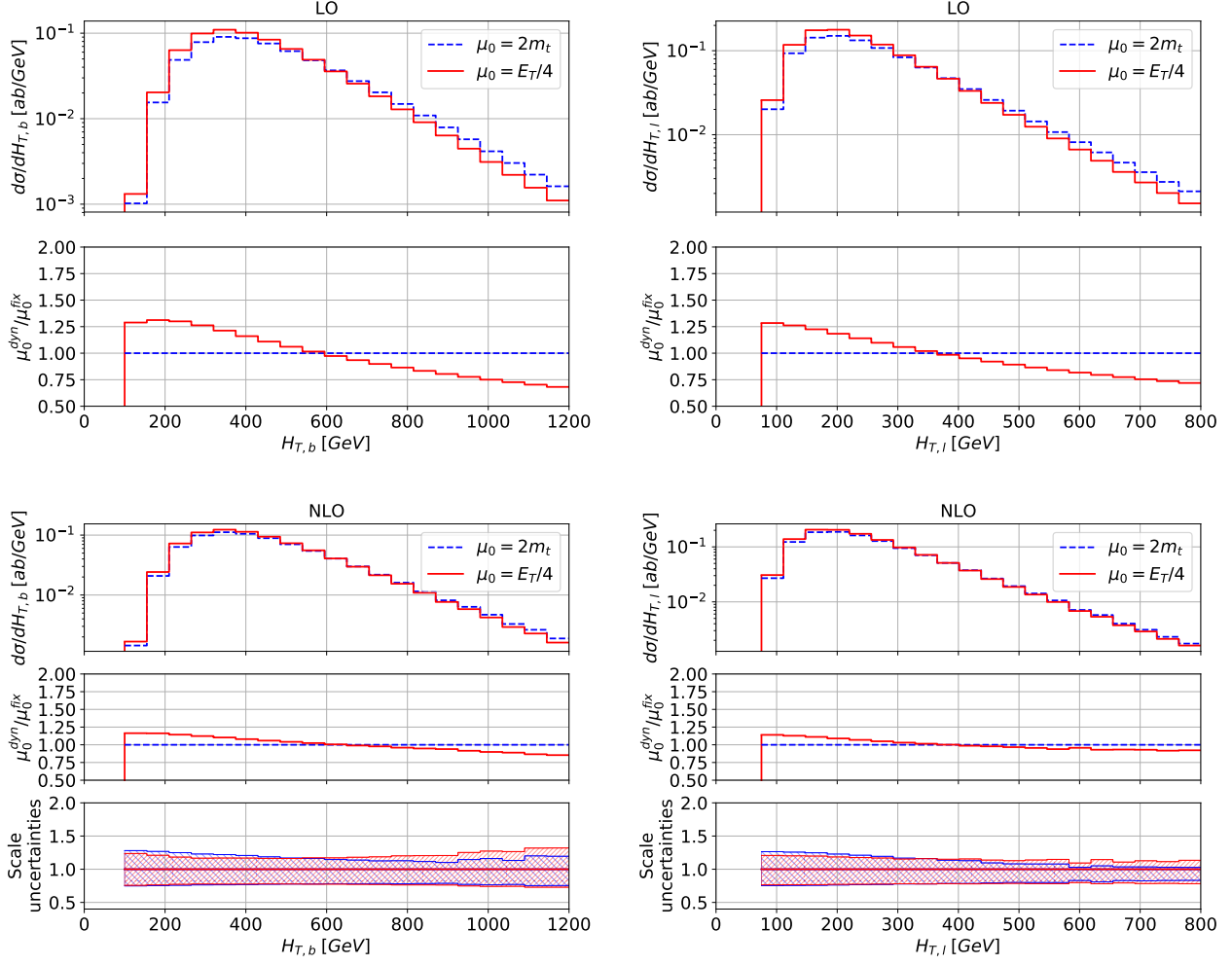


Figure 3: Differential cross-section distributions for $H_{T,b}$ and $H_{T,l}$ for the $pp \rightarrow t\bar{t}t + X$ process in the $3l$ decay channel at the LHC with $\sqrt{s} = 13.6$ TeV. The upper panels display the absolute (N)LO predictions for $\mu_0 = 2m_t$ and $\mu_0 = E_T/4$. The lower (middle) panels illustrate ratios to the result with $\mu_0 = 2m_t$. For the NLO case, the absolute magnitude of the scale uncertainty for both scale settings is also shown in the bottom panels. All results are presented with $|M_{jj} - m_W| < Q_{cut} = 25$ GeV and for the (N)LO MSHT20 PDF set.

sum of the transverse momenta of all charged leptons, $H_{T,\ell}$, defined according to

$$H_{T,b} = \sum_{i=1}^4 p_{T,b_i}, \quad H_{T,\ell} = \sum_{i=1}^3 p_{T,\ell_i}. \quad (5.1)$$

At NLO in QCD, the potential 5-th (hardest) b -jet, even if resolved and passed all the cuts, is not taken into account in the definition of $H_{T,b}$ to ensure that the same observable is considered at LO and NLO. Otherwise, one would expect large shape differences for this observable at the NLO QCD level. The upper panels display the absolute LO and NLO predictions for $\mu_0 = 2m_t$ and $\mu_0 = E_T/4$, while the lower panels illustrate the corresponding ratios to the results obtained with $\mu_0 = 2m_t$. In addition, for the NLO case only, additional panels emphasise the absolute magnitude of scale uncertainties for both scale choices. At LO, significant shape distortions up to even 60% are evident for both observables.

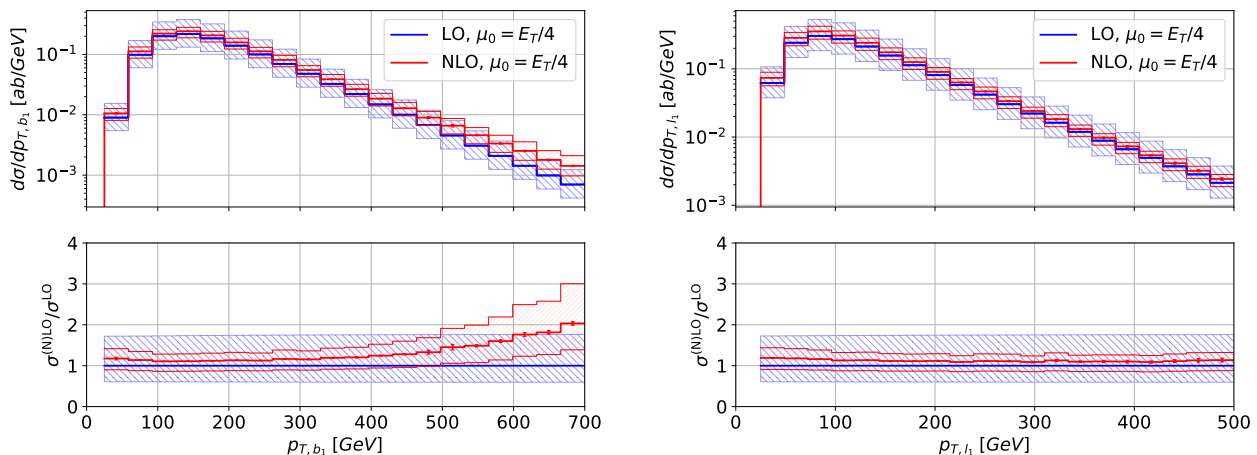


Figure 4: Differential cross-section distributions for p_{T,b_1} and p_{T,ℓ_1} for the $pp \rightarrow t\bar{t}t + X$ process in the 3ℓ decay channel at the LHC with $\sqrt{s} = 13.6$ TeV. Results are shown for $\mu_0 = E_T/4$ with $|M_{jj} - m_W| < Q_{cut} = 25$ GeV and for the (N)LO MSHT20 PDF set. The upper panels show the absolute (N)LO results. The lower panels present the differential \mathcal{K} -factors together with their uncertainty bands and the relative scale uncertainties of the LO cross sections. Monte Carlo errors are also displayed.

This confirms the well-known fact that LO predictions are very sensitive to the scale choice. However, as illustrated in the middle panels of the NLO plots, these large differences are mitigated when higher-order effects are included. Focusing now on the bottom panels of the NLO predictions, we can also observe that the scale uncertainties are of the order of 20% – 25%. More interestingly, both scale settings behave very similarly within the plotted range. A comparable pattern has been observed for most of the observables we examined. Contrary to the expectations, the fixed scale setting is also sufficient to describe differential cross-sectional distributions. This is due to the very large center-of-mass energy that is required to produce four tops, indicating that even higher- p_T tails beyond the TeV range are needed to find potential differences. Such phase-space regions, however, would not be accessible at the LHC. Since both scale settings produce similar results, we use the dynamic scale setting for the remaining distributions, keeping in mind that the differential cross-section results for the two scale choices are consistent with each other within their corresponding theoretical errors.

In Figure 4 we show the transverse momentum of the hardest b -jet, p_{T,b_1} , and the transverse momentum of the hardest charged lepton, p_{T,ℓ_1} . The upper panels display absolute LO and NLO predictions, including theoretical uncertainties. The lower panels show the differential \mathcal{K} -factors together with their uncertainty bands and the relative scale uncertainties of the LO cross sections. Even with $Q_{cut} = 25$ GeV, the higher-order QCD effects for p_{T,b_1} can be notably large in the tail of the distribution, reaching values up to even 100%. Moreover, in this phase-space region, the NLO result lies outside the LO uncertainty bands. In addition, the size of the NLO scale uncertainties increases significantly and becomes comparable to the size of the LO scale uncertainties. The QCD corrections for p_{T,ℓ_1} , on the other hand, are less pronounced, with the differential \mathcal{K} factor in the range of 1.10 – 1.20.

In Figure 5 we present additional observables related to the kinematics of the b -jets and charged leptons. We plot the average invariant mass of the two b -jets, $(M_{bb})_{avg}$, the transverse momentum of the system of the four hardest b -jets, $p_{T,b_1b_2b_3b_4}$, and the azimuthal angle between the two hardest charged leptons, $\Delta\phi_{l_1l_2}$. In general, we could observe that all observables associated with b -jets are more sensitive to higher-order QCD corrections, while those constructed of charged leptons are less

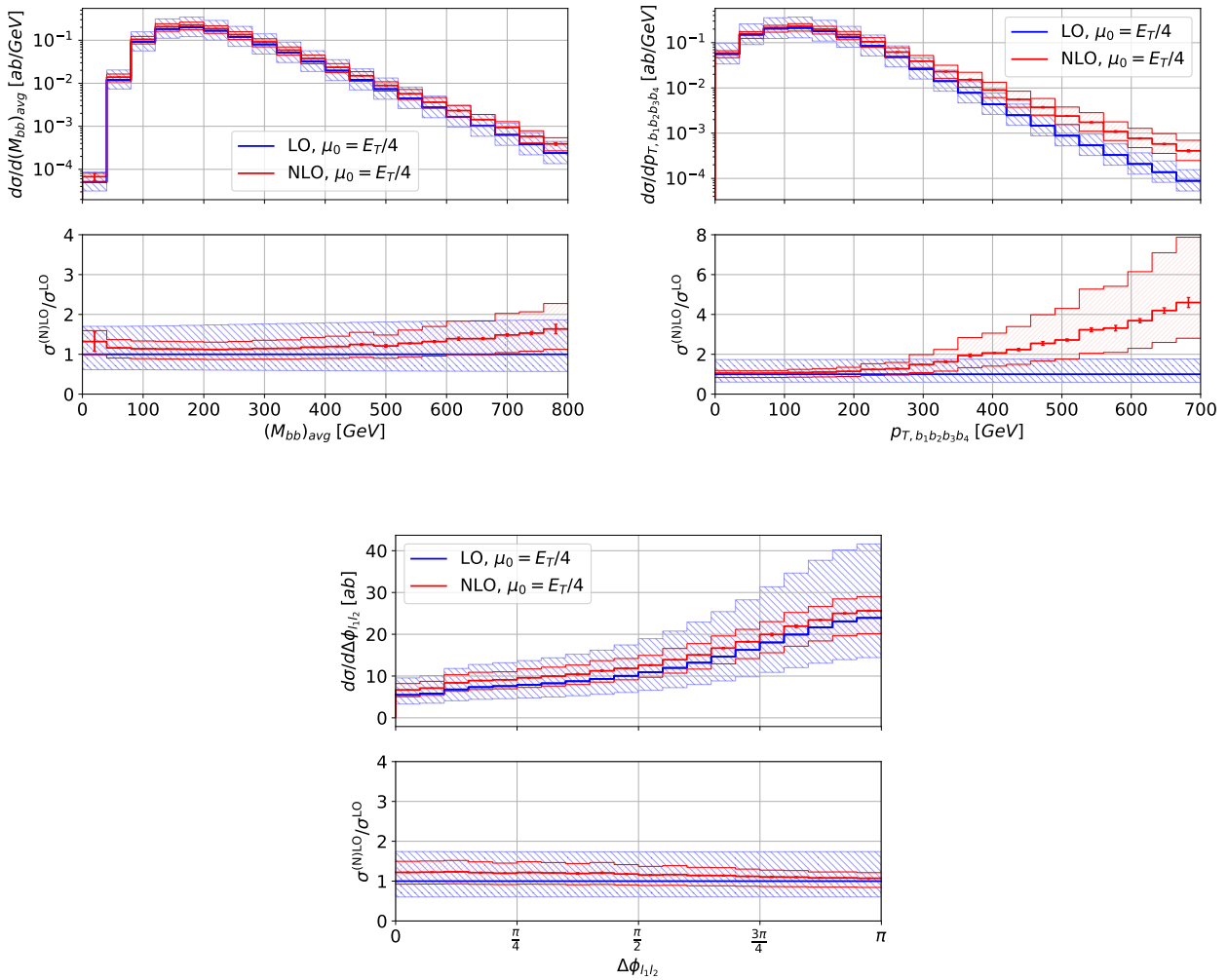


Figure 5: Same as Figure 4 but for the observables $(M_{bb})_{avg}$, $p_{T, b_1 b_2 b_3 b_4}$ and $\Delta\phi_{l_1 l_2}$.

susceptible. Specifically, for both $(M_{bb})_{avg}$ and $p_{T, b_1 b_2 b_3 b_4}$, NLO QCD corrections become significant in the tails of the distributions, reaching values of up to 65% and 360%, respectively. For $(M_{bb})_{avg}$, the NLO scale uncertainties are of the order of 40% in the distribution's tail, where additionally the NLO predictions are within the LO uncertainty bands. For the $p_{T, b_1 b_2 b_3 b_4}$ observable, NLO predictions lie almost entirely outside of the LO uncertainty bands. Moreover, the NLO uncertainties grow rapidly in the tails of the distribution. The gigantic \mathcal{K} -factor, which is also present in the 4ℓ decay channel, can be attributed to the presence of a highly energetic light jet emitted during the production stage, which recoils against the system of four top quarks (the system of four b -jets). For the dimensionless observable $\Delta\phi_{l_1 l_2}$, the size of the NLO QCD corrections ranges between 1% – 20%. To summarize this part, we can note that, on the one hand, the kinematics of the three charged leptons are very similar to the corresponding kinematics in the 4ℓ decay channel [29]. Indeed, for leptonic observables, the NLO QCD corrections are relatively small and the NLO predictions fall within the corresponding LO uncertainty bands. Nevertheless, there are some exceptions, e.g. the transverse momentum of the $l_1 l_2 l_3$ system or the total missing transverse momentum from the three neutrinos, where large QCD corrections are obtained in the tails. Similar effects have already been observed for these observables

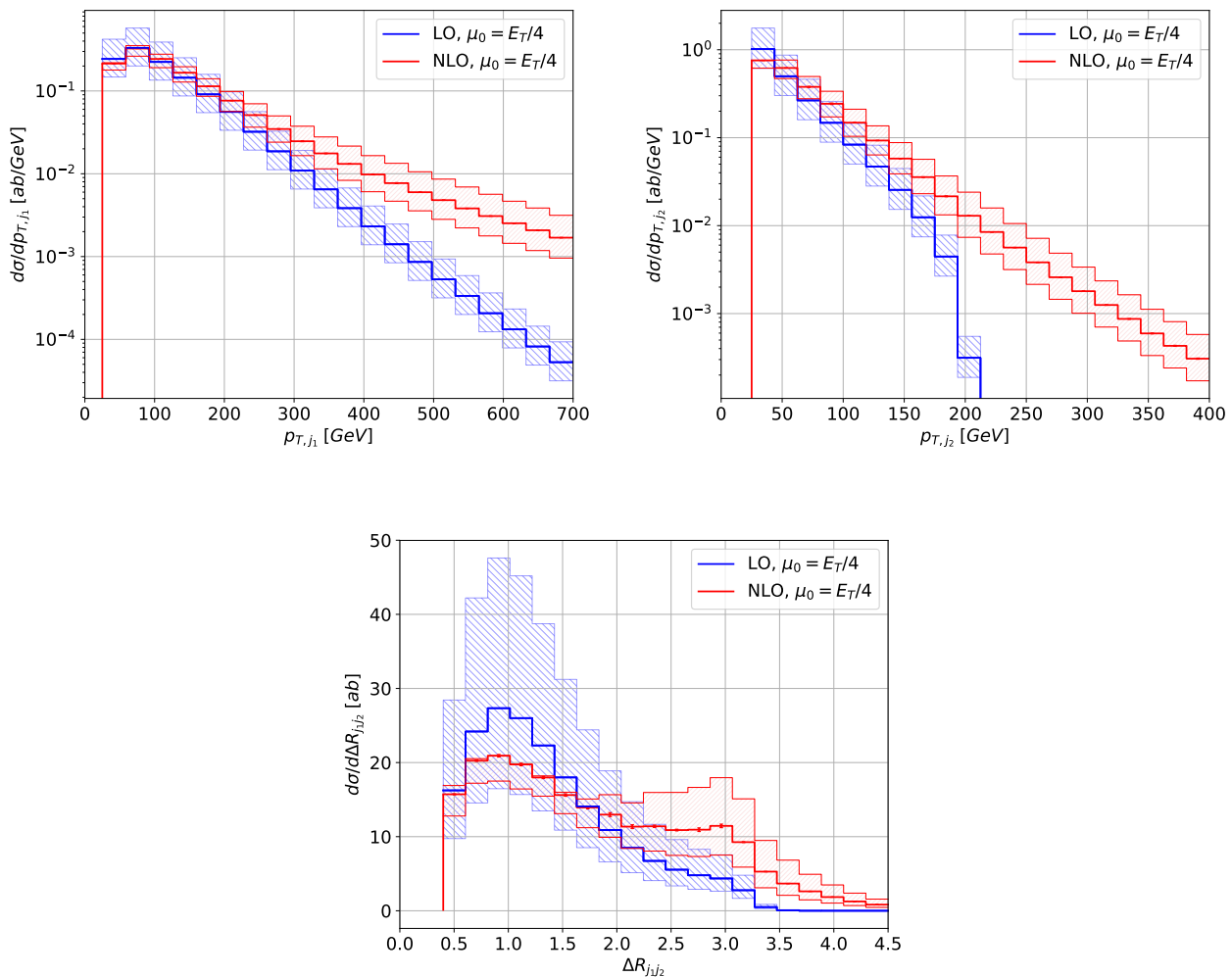


Figure 6: Differential cross-section distributions for p_{T,j_1} , p_{T,j_2} and $\Delta R_{j_1 j_2}$ for the $pp \rightarrow t\bar{t}\bar{t} + X$ process in the 3ℓ decay channel at the LHC with $\sqrt{s} = 13.6$ TeV. The (N)LO results, along with their uncertainties due to scale variation, are shown for $\mu_0 = E_T/4$ with $|M_{jj} - m_W| < Q_{cut} = 25$ GeV and for the (N)LO MSHT20 PDF set. Monte Carlo errors are also displayed.

in the 4ℓ decay channel. On the other hand, the observables involving b -jets are uniformly affected by much larger higher-order QCD effects compared to the 4ℓ decay channel.

In the 3ℓ decay channel, we observe significant shape distortions between the LO and NLO differential cross-section distributions for certain types of observables that involve the light jets. To illustrate this, in Figure 6 and Figure 7 we present the transverse momentum of the first and the second hardest light jet, p_{T,j_1} and p_{T,j_2} respectively, the angular distance (or angular separation) in the rapidity-azimuthal angle ($y-\phi$) phase space between the first and second hardest light jets, $\Delta R_{j_1 j_2}$, the invariant mass of the hardest light and b -jet, $M_{j_1 b_1}$, the azimuthal angle separation between the first and the second hardest light jet, $\Delta\phi_{j_1 j_2}$ and the rapidity of the hardest light jet, y_{j_1} . We emphasize that the differential \mathcal{K} -factors are not shown in Figure 6. This is due to the fact that for p_{T,j_1} , p_{T,j_2} and $\Delta R_{j_1 j_2}$ these factors become too large, which makes the results difficult to read. Therefore, we decided not to include them in these cases. For p_{T,j_1} , notable shape distortions are observed at NLO in QCD, especially towards the tail of the distribution. Again, they are caused by the presence of an

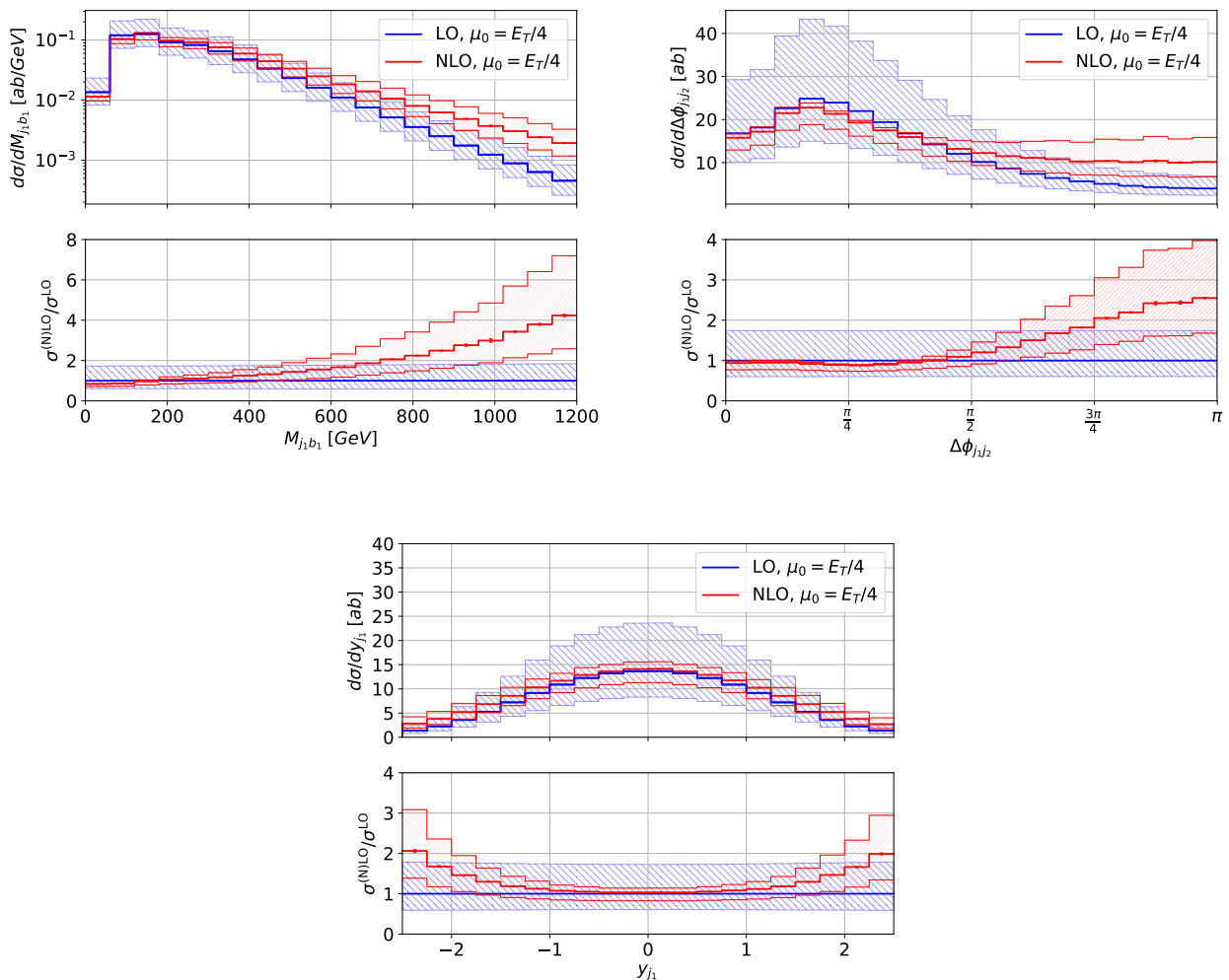


Figure 7: Same as Figure 6 but for the following observables: $M_{j_1 b_1}$, $\Delta\phi_{j_1 j_2}$ and y_{j_1} . The lower panels present the differential K -factors together with their uncertainty bands and the relative scale uncertainties of the LO cross sections.

additional high-energetic jet originating from the production stage of the $pp \rightarrow t\bar{t}t + X$ process. This extra light jet can attain large p_T values and emerge as either the hardest or second-hardest light jet. On the contrary, large values of p_{T,j_1} are strongly suppressed at LO by the kinematics of the W gauge boson. These constraints are particularly evident for p_{T,j_2} , where at LO there is a cut around 200 GeV which can be calculated from

$$(p_{T,j_2})_{max} \approx \frac{m_W}{(\Delta R_{j_1 j_2})_{min}} \approx 200 \text{ GeV}. \quad (5.2)$$

A similar cut can also be derived for the hardest light jet

$$(p_{T,j_1})_{max} \approx \frac{m_W^2}{(p_{T,j_2})_{min} (\Delta R_{j_1 j_2})_{min}^2} \approx 1615 \text{ GeV}. \quad (5.3)$$

However, this particular value is well outside the plotted range shown for p_{T,j_1} . Moreover, NLO

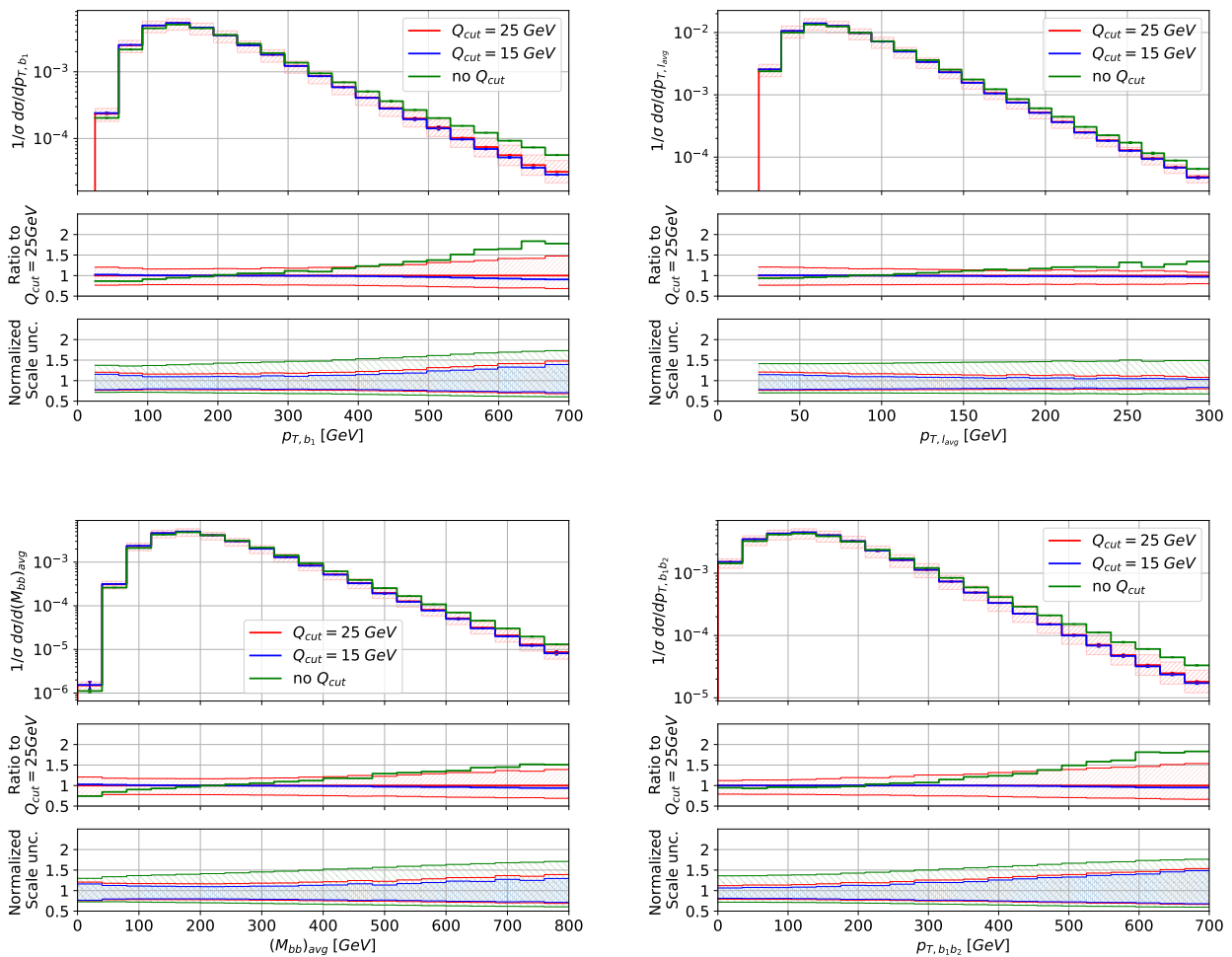


Figure 8: Normalized differential cross-section distributions for p_{T,b_1} , $p_{T,\ell_{avg}}$, $(M_{bb})_{avg}$ and p_{T,b_1b_2} , for the $pp \rightarrow t\bar{t}\bar{t} + X$ process in the 3ℓ decay channel at the LHC with $\sqrt{s} = 13.6$ TeV for three different scenarios of the $|M_{jj} - m_W| < Q_{cut}$ cut: $Q_{cut} = 15, 25$ GeV and $Q_{cut} \rightarrow \infty$, the latter case is labeled as no Q_{cut} . Results are given for $\mu_0 = E_T/4$ and the NLO MSHT20 PDF set. The upper panels show the normalised NLO predictions for the three cases including the scale uncertainties for the $Q_{cut} = 25$ GeV case. The middle panels present the ratios to the default case along with its uncertainties. The bottom panels display the size of the normalised NLO scale uncertainties for the three results.

scale uncertainties for both observables increase significantly at high- p_T tails. They are similar in magnitude or even larger than the corresponding LO uncertainties, which highlights the fact that in these phase-space regions, these observations only have LO accuracy. At NLO, significant changes in the shape of the $\Delta R_{j_1j_2}$ distribution are also visible. In particular, while at LO there is a single peak around $\Delta R_{j_1j_2} \approx 1$, at NLO we notice the appearance of a second peak near $\Delta R_{j_1j_2} \approx 3$. As a result, substantial higher-order QCD corrections are evident across the entire plotted range. Again, this is due to the additional light jet emitted at the production stage that breaks the LO kinematical restriction which favors $\Delta R_{j_1j_2} \approx 1$. Therefore, as expected, in the phase-space regions where two light jets are produced in a back-to-back configuration, which are described by LO-like dynamics, the magnitude of the NLO scale uncertainties exceeds the magnitude of the LO scale uncertainties, reaching values of up to 60%.

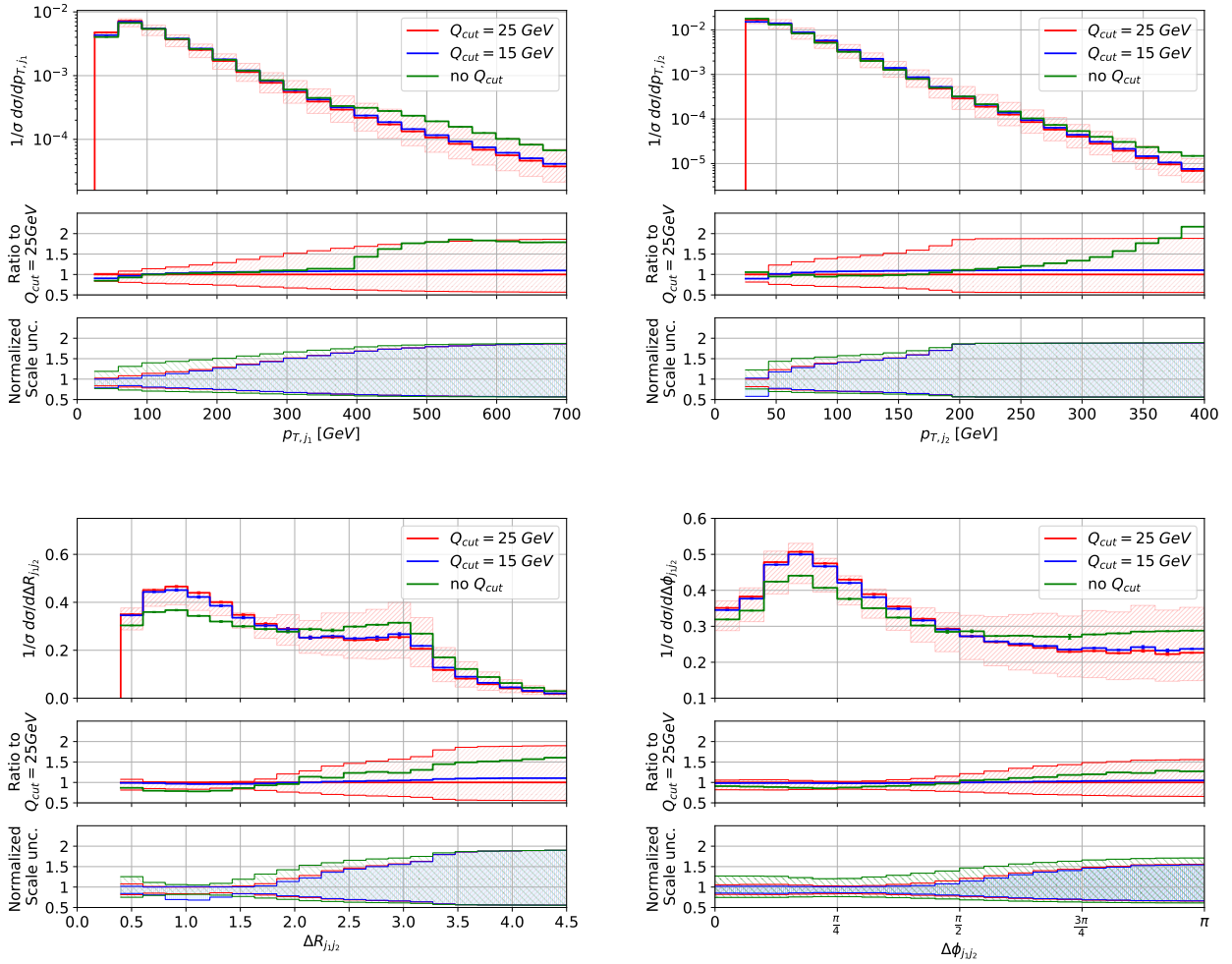


Figure 9: Same as Figure 8 but for the observables p_{T,j_1} , p_{T,j_2} , $\Delta R_{j_1j_2}$ and $\Delta\phi_{j_1j_2}$.

For the invariant mass of the hardest light and b -jet, we can observe that higher-order QCD corrections become very large in the tail of the distribution, where the \mathcal{K} -factor can exceed the value of 4. In addition, the magnitude of the NLO theoretical uncertainties in these phase-space regions is substantial, of the order of 70%. To explain the size of the large \mathcal{K} -factors, we note that at LO, in the rest frame of the (anti-)top quark, the maximum transverse momentum of the resulting b -jet is given by

$$(p_{T,b})_{max} = \frac{(m_t^2 - m_W^2)}{2m_t} \approx 67.5 \text{ GeV}. \quad (5.4)$$

Given that the majority of (anti-)top quarks are produced near the $4m_t$ threshold, pure kinematics imply that events above the value of

$$(M_{j_1b_1})_{max} \approx 2 \left((p_{T,b})_{max} (p_{T,j_1})_{max} \right)^{1/2} \approx 660 \text{ GeV}, \quad (5.5)$$

are kinematically strongly disfavored at LO. The absence of such a restriction at NLO explains the sharp rise in the \mathcal{K} -factor roughly above this value. Finally, the azimuthal angle between the first and second hardest jet receives large NLO QCD corrections up to 160% in the phase-space region where $\Delta\phi_{j_1j_2} \approx \pi$, while for the last observable y_{j_1} we notice NLO QCD corrections up to 100% near

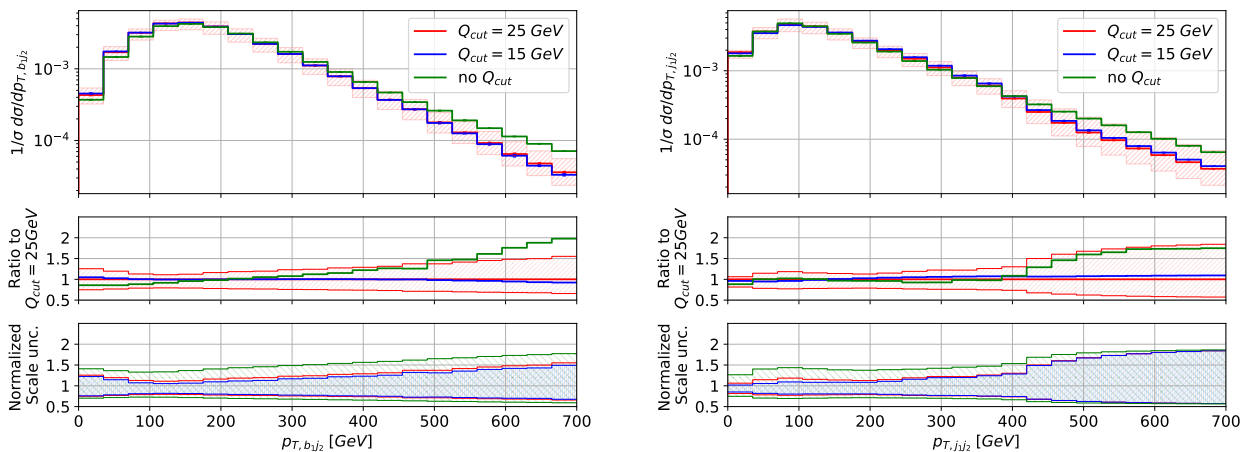


Figure 10: Same as Figure 8 but for the observables $p_{T, b_1 j_2}$ and $p_{T, j_1 j_2}$.

$|y_{j_1}| \approx 2.5$.

All the results presented so far in this Section have been obtained with $|M_{jj} - m_W| < Q_{cut} = 25$ GeV. However, we would like to study the effect of changing Q_{cut} also at the differential cross-section level. As a reminder, at the integrated cross-section level, our results strongly depended on the value of the parameter Q_{cut} , with higher values of Q_{cut} resulting in much larger cross sections. In the following, we study three different scenarios: $Q_{cut} = 15, 25$ GeV and the case with no restriction at all on M_{jj} , labelled as no Q_{cut} or the $Q_{cut} \rightarrow \infty$ case. Furthermore, due to large differences in normalization, we only analyse normalized differential cross-section distributions. In this way, we shall identify potential shape distortions, which can be very important for many experimental analyses targeting the $pp \rightarrow t\bar{t}j$ process in the 3ℓ decay channel.

In Figure 8 we present the transverse momentum of the hardest b -jet, p_{T, b_1} , the averaged transverse momentum of the lepton, $p_{T, \ell_{avg}}$, the averaged invariant mass of the two b -jet system, $(M_{bb})_{avg}$, and the transverse momentum of the system comprising the first and second hardest b -jets, $p_{T, b_1 b_2}$. In each case, the upper panels show the normalised NLO predictions for $Q_{cut} = 15, 25$ GeV and $Q_{cut} \rightarrow \infty$, including the scale uncertainties for the $Q_{cut} = 25$ GeV case. The middle panels present the ratios to the default case along with their uncertainties. The bottom panels display the size of the normalised NLO scale uncertainties for the three results. In all four cases, large shape distortions can be observed in the tails of the distributions when $Q_{cut} \rightarrow \infty$. In these phase-space regions the central predictions for the no Q_{cut} case are not even within the uncertainty bands of the default results, resulting in differences up to 80% for p_{T, b_1} and $p_{T, b_1 b_2}$, 50% for $(M_{bb})_{avg}$ and 30% for $p_{T, \ell_{avg}}$. When it comes to comparing the results for $Q_{cut} = 15$ GeV and $Q_{cut} = 25$ GeV, we note that their normalized predictions agree very well with each other and no significant distortion can be observed. Another important observation is the significant reduction in the size of the scale uncertainties for $Q_{cut} = 15, 25$ GeV. This reduction is evident throughout the plotted range of all distributions. Specifically, at the beginning of the spectrum, the scale uncertainties for the scenario without Q_{cut} reach 35% – 45%, while when $Q_{cut} = 15, 25$ GeV is applied, the corresponding uncertainties vary between 15% – 25% only. On the other hand, in the tails of these distributions, we can observe uncertainties of the order of 50% – 80% for the $Q_{cut} \rightarrow \infty$ case.

In Figure 9, we show additional cross-section distributions focusing this time on the kinematics of the light jets. We display anew $p_{T, j_1}, p_{T, j_2}, \Delta R_{j_1 j_2}$ and $\Delta\phi_{j_1 j_2}$. Also here there are minimal differences

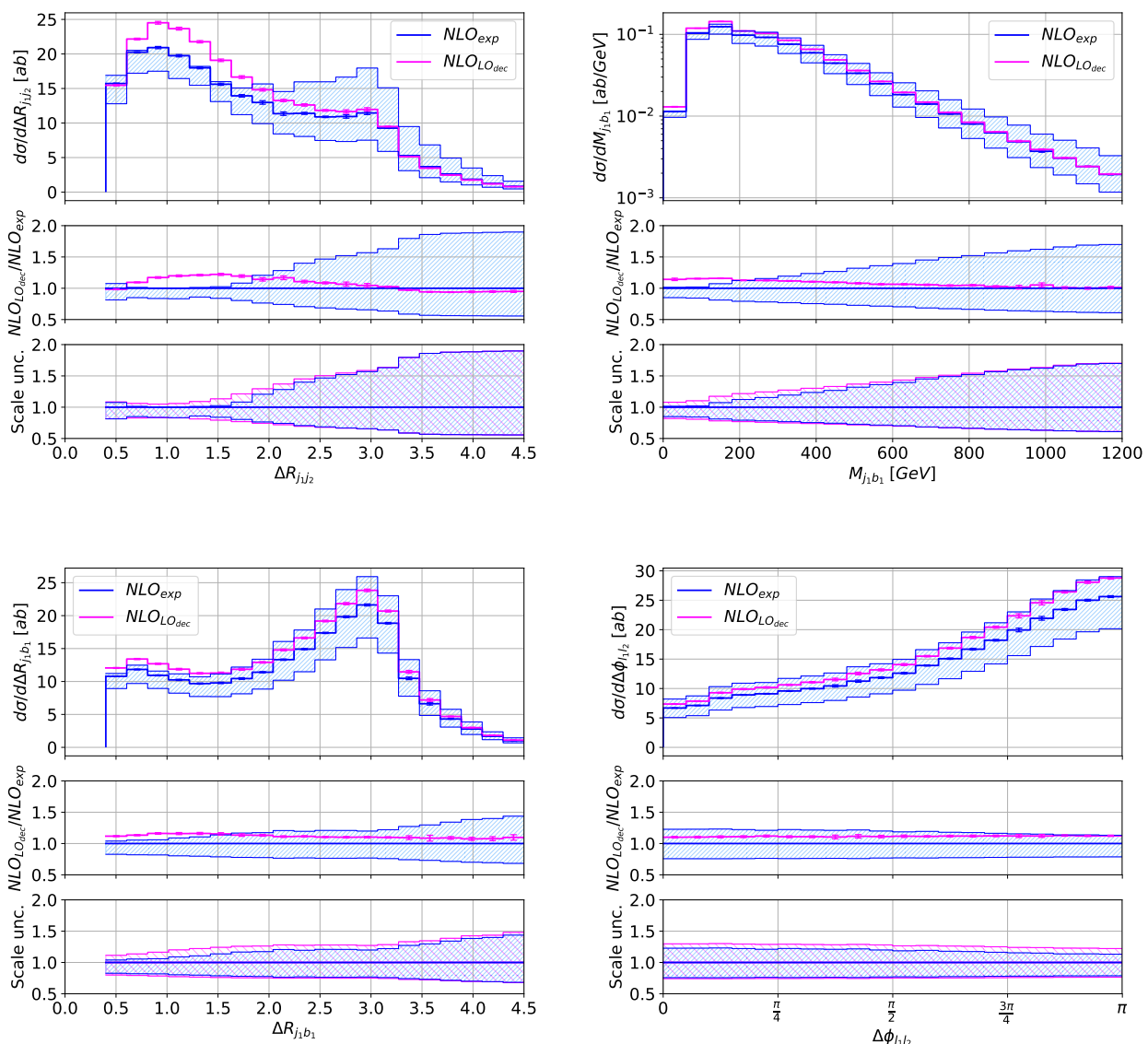


Figure 11: NLO differential cross-section distributions for $d\sigma_{\text{exp}}^{\text{NLO}}/dX$ and $d\sigma_{\text{LOdec}}^{\text{NLO}}/dX$, where $X = \Delta R_{j_1j_2}, M_{j_1b_1}, \Delta R_{j_1b_1}, \Delta\phi_{\ell_1\ell_2}$ for the $pp \rightarrow t\bar{t}t + X$ process in the 3ℓ decay channel at the LHC with $\sqrt{s} = 13.6$ TeV. Results are shown for $\mu_0 = E_T/4$ with $|M_{jj} - m_W| < Q_{\text{cut}} = 25$ GeV and for the NLO MSHT20 PDF set. The upper panels display the absolute NLO predictions for $d\sigma_{\text{exp}}^{\text{NLO}}/dX$ and $d\sigma_{\text{LOdec}}^{\text{NLO}}/dX$ together with the scale uncertainties of the $d\sigma_{\text{exp}}^{\text{NLO}}/dX$ case. The middle panels illustrate the corresponding ratio to $d\sigma_{\text{exp}}^{\text{NLO}}/dX$. The bottom panels provide the size of the scale uncertainties for both cases normalized to their corresponding NLO results. Monte Carlo errors are also displayed.

between the two cases with $Q_{\text{cut}} = 15$ GeV and $Q_{\text{cut}} = 25$ GeV. On the other hand, the predictions for the scenario with no restriction on M_{jj} tend to increase in the tails of the dimensionful observables. However, such predictions are still within the range of the large NLO uncertainty bands observed in these phase-space regions. The only exception is the last bin of the p_{T,j_2} observable. For the angular separation between the two hardest light jets we observe differences of up to 20% in the region near $\Delta R_{j_1j_2} \approx 1$, where most of the events are concentrated. In addition, the result without Q_{cut} lies outside the uncertainty bands of the default case. Finally, for both observables $\Delta R_{j_1j_2}$ and $\Delta\phi_{j_1j_2}$ the

difference between the $Q_{cut} \rightarrow \infty$ case and the other two predictions are substantial for $\Delta R_{j_1 j_2} \gtrsim 3$ and $\Delta\phi_{j_1 j_2} > \pi/2$. Still, the result without the Q_{cut} cut is within the large NLO uncertainties that are LO-like for these phase-space regions. It is worth noting that the size of the scale uncertainties tends to be consistent for the three different scenarios in the phase-space regions where the NLO predictions are mainly driven by the LO dynamics, and is significantly reduced for low values of p_T , $\Delta R_{j_1 j_2} < 3$ and $\Delta\phi_{j_1 j_2} < \pi/2$, when Q_{cut} is applied.

In Figure 10 we display $p_{T, j_1 j_2}$ and $p_{T, b_1 j_2}$. These two observables are closely related because in the case of potential misidentification of b - and light-jets, $p_{T, b_1 j_2}$ can be interpreted as $p_{T, j_1 j_2}$. For the $Q_{cut} \rightarrow \infty$ case shape distortions are evident in both observables, but they are more pronounced for $p_{T, b_1 j_2}$, where the ratio to the default case of $Q_{cut} = 25$ GeV approaches 2 in the tail of the distribution.

So far, we have observed significant shape distortions in almost all observables we have studied when the M_{jj} cut is not applied. We have also verified that these distortions are less evident for the dimensionless observables that do not involve light jets in their definition. Furthermore, the size of the scale uncertainties is significantly larger in the $Q_{cut} \rightarrow \infty$ scenario. Thus, restricting the value of M_{jj} may prove beneficial for increasing the efficiency of future experimental analyses targeting the 3ℓ channel.

In the last step, we examine the differences between $d\sigma_{\text{exp}}^{\text{NLO}}/dX$ and $d\sigma_{\text{LOdec}}^{\text{NLO}}/dX$ theoretical predictions for $X = \Delta R_{j_1 j_2}, M_{j_1 b_1}, \Delta R_{j_1 b_1}, \Delta\phi_{l_1 l_2}$. In this way, we wish to assess the importance of higher-order effects in top-quark decays also at the differential cross-section level. In Figure 11 we present these results for the default $|M_{jj} - m_W| < Q_{cut} = 25$ GeV cut. The upper panels display the absolute predictions for $d\sigma_{\text{exp}}^{\text{NLO}}/dX$ and $d\sigma_{\text{LOdec}}^{\text{NLO}}/dX$ along with the scale uncertainties of the $d\sigma_{\text{exp}}^{\text{NLO}}/dX$ result. The middle panels illustrate the ratios to $d\sigma_{\text{exp}}^{\text{NLO}}/dX$ including the scale uncertainties of the expanded predictions. The bottom panels give the size of the scale uncertainties for both cases normalized to the respective NLO values. Large differences up to 22% are observed for the angular separation between the two hardest light jets for $\Delta R_{j_1 j_2} \approx 1$. In these phase-space regions the $d\sigma_{\text{LOdec}}^{\text{NLO}}$ theoretical predictions lie outside the uncertainty bands of the default case. The latter uncertainties are of the order of 13%. The observables $M_{j_1 b_1}$ and $\Delta R_{j_1 b_1}$ show smaller differences between the two NWA cases. Still in some phase-space regions, i.e. for $M_{j_1 b_1} \leq 200$ GeV and for $\Delta R_{j_1 b_1} \in (0.4, 1.5)$, the $d\sigma_{\text{LOdec}}^{\text{NLO}}/dX$ predictions are not within the scale uncertainty bands of $d\sigma_{\text{exp}}^{\text{NLO}}/dX$, which are of the order of 20%. The opposite is true for $\Delta\phi_{l_1 l_2}$ that show consistent differences of the order of 10%. Furthermore, these effects are within the theoretical uncertainties of the expanded result, which do not exceed 25%. When analyzing the lower panels of Figure 11 we notice a universal behavior. Scale uncertainties decrease when QCD corrections are properly accounted for in both the production and decay stages of four top quarks. The only exceptions are the phase-space regions where the NLO QCD uncertainties for $d\sigma_{\text{exp}}^{\text{NLO}}/dX$ are very large and where the theoretical errors of both NWA approaches are of the same size.

6 Summary and Outlook

In this paper we presented a comprehensive NLO QCD analysis of the $pp \rightarrow t\bar{t}\bar{t} + X$ process in the 3ℓ decay channel at the LHC with $\sqrt{s} = 13.6$ TeV. We provided our NLO QCD predictions both at the integrated and differential (fiducial) cross-section level utilising the NWA methods. Specifically, we studied the so-called full NWA, the expanded version of the NWA and the case where the NLO QCD corrections are present only in the production stage of the $t\bar{t}\bar{t}$ process. In addition, we considered different scale choices and PDF sets in our studies. We showed the need to use the $|M_{jj} - m_W| < Q_{cut}$ cut to restore perturbative convergence in the calculations of the higher-order QCD corrections for

the current process and argued that $Q_{cut} = 25$ GeV is a very well-motivated choice. With our input parameters and the set of selection cuts, as well as for $|M_{jj} - m_W| < 25$ GeV we observed that the magnitude of the NLO QCD corrections strongly depends on the choice of the LO PDF set, and in particular on the $\alpha_s(m_Z)$ value used there. Accordingly, the \mathcal{K} -factors defined as $\mathcal{K} = \sigma_{\text{exp}}^{\text{NLO}}/\sigma^{\text{LO}}$ are within the range of $\mathcal{K} \in (1.08 - 1.37)$. However, at the NLO level in QCD, theoretical predictions for various PDF sets agree with each other at the 1σ level, separately for $\mu_0 = 2m_t$ and $\mu_0 = E_T/4$. In addition, the PDF and scale uncertainties are independent of the scale setting and are of the order of 2% – 6% and 23%, respectively. The various NWA models we included in our study provided us with additional information. In particular, we established that neglecting higher-order QCD corrections in top-quark decays resulted in an overestimation of the cross section by about 11% – 12%, depending on the renormalisation and factorisation scale chosen, and led to an increase in scale uncertainties from 23% to 26%. On the other hand, the difference between $\sigma_{\text{full}}^{\text{NLO}}$ and $\sigma_{\text{exp}}^{\text{NLO}}$ is at the 12% – 13% level, thus, well within the stated theoretical uncertainties. In addition, when moving from $\sigma_{\text{exp}}^{\text{NLO}}$ to $\sigma_{\text{full}}^{\text{NLO}}$, theoretical uncertainties are reduced from 23% to 19%. Furthermore, we investigated the dependence of NLO QCD results on the Q_{cut} used. We observed a high sensitivity of the \mathcal{K} factor on the choice of Q_{cut} . In particular, in the most extreme case, i.e., for $Q_{cut} \rightarrow \infty$, we obtained not only significant theoretical uncertainties, up to even 45%, but also higher-order QCD effects of the order of 80% – 130%.

At the differential (fiducial) cross-section level even with the $|M_{jj} - m_W| < 25$ GeV cut, we observed giant differential \mathcal{K} -factors and huge shape distortions between the LO and NLO results for certain types of observables that are associated with light jets. Such effects are caused by the presence of an additional jet coming from the production stage of the $pp \rightarrow t\bar{t}\bar{t} + X$ process, which can reach large p_T values and appear as the hardest or second-hardest light jet. Moreover, it can mimic one of the decay products of the W boson. In addition, we studied the effect of changing Q_{cut} on the differential cross-section distributions. We examined the following three cases: $Q_{cut} = 15$ GeV, 25 GeV and the $Q_{cut} \rightarrow \infty$ case. For all observables considered, the normalized predictions for $Q_{cut} = 15$ GeV and $Q_{cut} = 25$ GeV agreed very well with each other and no significant distortion could be observed. On the other hand, large shape distortions could be detected in the tails of the dimensionful distributions when $Q_{cut} \rightarrow \infty$. This was true even for some angular distributions. In a final step, to estimate the size of higher-order QCD effects in top-quark decays, we compared $d\sigma_{\text{exp}}^{\text{NLO}}/dX$ and $d\sigma_{\text{LO}_{\text{dec}}}^{\text{NLO}}/dX$. We observed significant differences for both dimensionless and dimensionful observables. Moreover, for some observables, these shape distortions were not covered by the theoretical uncertainties.

In summary, higher-order corrections are undoubtedly required for the $pp \rightarrow t\bar{t}\bar{t} + X$ process in the 3ℓ decay channel at the LHC. They should be consistently included in both the production and decay stages of the $4t$ process as they impact not only the overall normalisation, but also the size of the theoretical uncertainties due to scale dependence. To control the size of NLO QCD corrections and theoretical uncertainties, the Q_{cut} cut is mandatory. We might add at this point that, for the High Luminosity Large Hadron Collider (HL-LHC) we expect $N \approx (150 - 200)$ events per experiment assuming $\ell^\pm = e^\pm, \mu^\pm$ only. Thus, the predicted uncertainties for this process, estimated solely on the basis of the integrated luminosity planned for the HL-LHC, which is $(3 - 4) \text{ ab}^{-1}$, and when combining the ATLAS and CMS results, are in the range of $\delta = 1/\sqrt{N} \in (6\% - 5\%)$. This further highlights the importance of precise calculations for this process.

Finally, it would be beneficial to compare NLO QCD results in the NWA to results obtained from the on-shell $pp \rightarrow t\bar{t}\bar{t}$ calculation, with approximate spin-correlations in top-quark and W decays, matched to parton showers. Such a comparison could assess to what extent parton-shower effects can reproduce all the contributions required at the NLO level in QCD for the $pp \rightarrow t\bar{t}\bar{t} + X$ process in

the 3ℓ decay channel. It would also help to identify phase-space regions and specific observables that are sensitive to parton-shower effects. In addition, we would be able to compare and thus verify the magnitude of the theoretical uncertainties arising from scale dependence. Such analyses and comparisons are already at an advanced stage.

Acknowledgments

This work was supported by the Deutsche Forschungsgemeinschaft (DFG) under grant 396021762 - TRR 257: *Particle Physics Phenomenology after the Higgs Discovery*, and grant 400140256 - GRK 2497: *The Physics of the Heaviest Particles at the LHC*.

Support by a grant of the Bundesministerium für Bildung und Forschung (BMBF) is additionally acknowledged.

The authors gratefully acknowledge the computing time provided to them at the NHR Center NHR4CES at RWTH Aachen University (project number p0020216). This is funded by the Federal Ministry of Education and Research, and the state governments participating on the basis of the resolutions of the GWK for national high performance computing at universities.

References

- [1] G. Bevilacqua and M. Worek, *Constraining BSM Physics at the LHC: Four top final states with NLO accuracy in perturbative QCD*, *JHEP* **07** (2012) 111 [[1206.3064](#)].
- [2] Q.-H. Cao, S.-L. Chen and Y. Liu, *Probing Higgs Width and Top Quark Yukawa Coupling from $t\bar{t}H$ and $t\bar{t}\bar{t}$ Productions*, *Phys. Rev. D* **95** (2017) 053004 [[1602.01934](#)].
- [3] Q.-H. Cao, S.-L. Chen, Y. Liu, R. Zhang and Y. Zhang, *Limiting top quark-Higgs boson interaction and Higgs-boson width from multitop productions*, *Phys. Rev. D* **99** (2019) 113003 [[1901.04567](#)].
- [4] M. Guchait, F. Mahmoudi and K. Sridhar, *Associated production of a Kaluza-Klein excitation of a gluon with a t anti- t pair at the LHC*, *Phys. Lett. B* **666** (2008) 347 [[0710.2234](#)].
- [5] A. Pomarol and J. Serra, *Top Quark Compositeness: Feasibility and Implications*, *Phys. Rev. D* **78** (2008) 074026 [[0806.3247](#)].
- [6] T. Plehn and T.M.P. Tait, *Seeking Sgluons*, *J. Phys. G* **36** (2009) 075001 [[0810.3919](#)].
- [7] S. Jung and J.D. Wells, *Low-scale warped extra dimension and its predilection for multiple top quarks*, *JHEP* **11** (2010) 001 [[1008.0870](#)].
- [8] T. Gregoire, E. Katz and V. Sanz, *Four top quarks in extensions of the standard model*, *Phys. Rev. D* **85** (2012) 055024 [[1101.1294](#)].
- [9] S. Calvet, B. Fuks, P. Gris and L. Valery, *Searching for sgluons in multitop events at a center-of-mass energy of 8 TeV*, *JHEP* **04** (2013) 043 [[1212.3360](#)].
- [10] C. Arina et al., *A comprehensive approach to dark matter studies: exploration of simplified top-philic models*, *JHEP* **11** (2016) 111 [[1605.09242](#)].
- [11] E. Alvarez, D.A. Faroughy, J.F. Kamenik, R. Morales and A. Szyrkman, *Four tops for LHC*, *Nucl. Phys. B* **915** (2017) 19 [[1611.05032](#)].
- [12] H. Baer, V. Barger, J.S. Gainer, P. Huang, M. Savoy, D. Sengupta et al., *Gluino reach and mass extraction at the LHC in radiatively-driven natural SUSY*, *Eur. Phys. J. C* **77** (2017) 499 [[1612.00795](#)].
- [13] H. Baer, V. Barger, J.S. Gainer, H. Serce and X. Tata, *Reach of the high-energy LHC for gluinos and top squarks in SUSY models with light Higgsinos*, *Phys. Rev. D* **96** (2017) 115008 [[1708.09054](#)].

- [14] E. Alvarez, A. Juste and R.M.S. Seoane, *Four-top as probe of light top-philic New Physics*, *JHEP* **12** (2019) 080 [[1910.09581](#)].
- [15] Anisha, O. Atkinson, A. Bhardwaj, C. Englert, W. Naskar and P. Stylianou, *BSM reach of four-top production at the LHC*, *Phys. Rev. D* **108** (2023) 035001 [[2302.08281](#)].
- [16] C. Degrande, J.-M. Gerard, C. Grojean, F. Maltoni and G. Servant, *Non-resonant New Physics in Top Pair Production at Hadron Colliders*, *JHEP* **03** (2011) 125 [[1010.6304](#)].
- [17] C. Zhang, *Constraining $q\bar{t}t$ operators from four-top production: a case for enhanced EFT sensitivity*, *Chin. Phys. C* **42** (2018) 023104 [[1708.05928](#)].
- [18] G. Banelli, E. Salvioni, J. Serra, T. Theil and A. Weiler, *The Present and Future of Four Top Operators*, *JHEP* **02** (2021) 043 [[2010.05915](#)].
- [19] R. Aoude, H. El Faham, F. Maltoni and E. Vryonidou, *Complete SMEFT predictions for four top quark production at hadron colliders*, *JHEP* **10** (2022) 163 [[2208.04962](#)].
- [20] ATLAS collaboration, *Evidence for $t\bar{t}\bar{t}\bar{t}$ production in the multilepton final state in proton–proton collisions at $\sqrt{s} = 13$ TeV with the ATLAS detector*, *Eur. Phys. J. C* **80** (2020) 1085 [[2007.14858](#)].
- [21] CMS collaboration, *Evidence for Four-Top Quark Production in Proton-Proton Collisions at $s=13$ TeV*, *Phys. Lett. B* **844** (2023) 138076 [[2303.03864](#)].
- [22] ATLAS collaboration, *Observation of four-top-quark production in the multilepton final state with the ATLAS detector*, *Eur. Phys. J. C* **83** (2023) 496 [[2303.15061](#)].
- [23] CMS collaboration, *Observation of four top quark production in proton-proton collisions at $\sqrt{s} = 13$ TeV*, *Phys. Lett. B* **847** (2023) 138290 [[2305.13439](#)].
- [24] J. Alwall, R. Frederix, S. Frixione, V. Hirschi, F. Maltoni, O. Mattelaer et al., *The automated computation of tree-level and next-to-leading order differential cross sections, and their matching to parton shower simulations*, *JHEP* **07** (2014) 079 [[1405.0301](#)].
- [25] F. Maltoni, D. Pagani and I. Tsinikos, *Associated production of a top-quark pair with vector bosons at NLO in QCD: impact on $t\bar{t}H$ searches at the LHC*, *JHEP* **02** (2016) 113 [[1507.05640](#)].
- [26] R. Frederix, D. Pagani and M. Zaro, *Large NLO corrections in $t\bar{t}W^\pm$ and $t\bar{t}\bar{t}$ hadroproduction from supposedly subleading EW contributions*, *JHEP* **02** (2018) 031 [[1711.02116](#)].
- [27] M. van Beekveld, A. Kulesza and L.M. Valero, *Threshold Resummation for the Production of Four Top Quarks at the LHC*, *Phys. Rev. Lett.* **131** (2023) 211901 [[2212.03259](#)].
- [28] T. Ježo and M. Kraus, *Hadroproduction of four top quarks in the powheg box*, *Phys. Rev. D* **105** (2022) 114024 [[2110.15159](#)].
- [29] N. Dimitrakopoulos and M. Worek, *Four top final states with NLO accuracy in perturbative QCD: 4 lepton channel*, [2401.10678](#).
- [30] V.S. Fadin, V.A. Khoze and A.D. Martin, *How suppressed are the radiative interference effects in heavy instable particle production?*, *Phys. Lett. B* **320** (1994) 141 [[hep-ph/9309234](#)].
- [31] G. Bevilacqua, H.B. Hartanto, M. Kraus, T. Weber and M. Worek, *Off-shell vs on-shell modelling of top quarks in photon associated production*, *JHEP* **03** (2020) 154 [[1912.09999](#)].
- [32] G. Bevilacqua, H.-Y. Bi, H.B. Hartanto, M. Kraus and M. Worek, *The simplest of them all: $t\bar{t}W^\pm$ at NLO accuracy in QCD*, *JHEP* **08** (2020) 043 [[2005.09427](#)].
- [33] D. Stremmer and M. Worek, *Production and decay of the Higgs boson in association with top quarks*, *JHEP* **02** (2022) 196 [[2111.01427](#)].
- [34] G. Bevilacqua, H.B. Hartanto, M. Kraus, J. Nasufi and M. Worek, *NLO QCD corrections to full off-shell production of $t\bar{t}Z$ including leptonic decays*, *JHEP* **08** (2022) 060 [[2203.15688](#)].

- [35] J. Hermann, D. Stremmer and M. Worek, *CP structure of the top-quark Yukawa interaction: NLO QCD corrections and off-shell effects*, *JHEP* **09** (2022) 138 [[2205.09983](#)].
- [36] A. Denner and M. Pellen, *Off-shell production of top-antitop pairs in the lepton+jets channel at NLO QCD*, *JHEP* **02** (2018) 013 [[1711.10359](#)].
- [37] G. Bevilacqua, M. Czakon, M.V. Garzelli, A. van Hameren, A. Kardos, C.G. Papadopoulos et al., *HELAC-NLO*, *Comput. Phys. Commun.* **184** (2013) 986 [[1110.1499](#)].
- [38] A. van Hameren, C.G. Papadopoulos and R. Pittau, *Automated one-loop calculations: A Proof of concept*, *JHEP* **09** (2009) 106 [[0903.4665](#)].
- [39] M. Czakon, C.G. Papadopoulos and M. Worek, *Polarizing the Dipoles*, *JHEP* **08** (2009) 085 [[0905.0883](#)].
- [40] G. Ossola, C.G. Papadopoulos and R. Pittau, *CutTools: A Program implementing the OPP reduction method to compute one-loop amplitudes*, *JHEP* **03** (2008) 042 [[0711.3596](#)].
- [41] G. Ossola, C.G. Papadopoulos and R. Pittau, *Reduction of one-loop amplitudes at the integrand level: NLO QCD calculations*, *Acta Phys. Polon. B* **39** (2008) 1685.
- [42] G. Ossola, C.G. Papadopoulos and R. Pittau, *On the Rational Terms of the one-loop amplitudes*, *JHEP* **05** (2008) 004 [[0802.1876](#)].
- [43] P. Draggiotis, M.V. Garzelli, C.G. Papadopoulos and R. Pittau, *Feynman Rules for the Rational Part of the QCD 1-loop amplitudes*, *JHEP* **04** (2009) 072 [[0903.0356](#)].
- [44] A. van Hameren, *OneLoop: For the evaluation of one-loop scalar functions*, *Comput. Phys. Commun.* **182** (2011) 2427 [[1007.4716](#)].
- [45] S. Catani and M.H. Seymour, *A General algorithm for calculating jet cross-sections in NLO QCD*, *Nucl. Phys. B* **485** (1997) 291 [[hep-ph/9605323](#)].
- [46] S. Catani, S. Dittmaier, M.H. Seymour and Z. Trocsanyi, *The Dipole formalism for next-to-leading order QCD calculations with massive partons*, *Nucl. Phys. B* **627** (2002) 189 [[hep-ph/0201036](#)].
- [47] G. Bevilacqua, M. Czakon, M. Kubocz and M. Worek, *Complete Nagy-Soper subtraction for next-to-leading order calculations in QCD*, *JHEP* **10** (2013) 204 [[1308.5605](#)].
- [48] A. van Hameren, *PARNI for importance sampling and density estimation*, *Acta Phys. Polon. B* **40** (2009) 259 [[0710.2448](#)].
- [49] A. van Hameren, *Kaleu: A General-Purpose Parton-Level Phase Space Generator*, [1003.4953](#).
- [50] Z. Nagy and Z. Trocsanyi, *Next-to-leading order calculation of four jet observables in electron positron annihilation*, *Phys. Rev. D* **59** (1999) 014020 [[hep-ph/9806317](#)].
- [51] Z. Nagy, *Next-to-leading order calculation of three jet observables in hadron hadron collision*, *Phys. Rev. D* **68** (2003) 094002 [[hep-ph/0307268](#)].
- [52] G. Bevilacqua, M. Czakon, C.G. Papadopoulos, R. Pittau and M. Worek, *Assault on the NLO Wishlist: $pp \rightarrow t\bar{t}b\bar{b}$* , *JHEP* **09** (2009) 109 [[0907.4723](#)].
- [53] M. Czakon, H.B. Hartanto, M. Kraus and M. Worek, *Matching the Nagy-Soper parton shower at next-to-leading order*, *JHEP* **06** (2015) 033 [[1502.00925](#)].
- [54] S. Badger, B. Biedermann and P. Uwer, *NGLuon: A Package to Calculate One-loop Multi-gluon Amplitudes*, *Comput. Phys. Commun.* **182** (2011) 1674 [[1011.2900](#)].
- [55] S. Actis, A. Denner, L. Hofer, J.-N. Lang, A. Scharf and S. Uccirati, *RECOLA: REcursive Computation of One-Loop Amplitudes*, *Comput. Phys. Commun.* **214** (2017) 140 [[1605.01090](#)].
- [56] J. Alwall et al., *A Standard format for Les Houches event files*, *Comput. Phys. Commun.* **176** (2007) 300 [[hep-ph/0609017](#)].
- [57] I. Antcheva et al., *ROOT: A C++ framework for petabyte data storage, statistical analysis and*

- visualization, *Comput. Phys. Commun.* **180** (2009) 2499 [[1508.07749](#)].
- [58] Z. Bern, L.J. Dixon, F. Febres Cordero, S. Höche, H. Ita, D.A. Kosower et al., *Ntuples for NLO Events at Hadron Colliders*, *Comput. Phys. Commun.* **185** (2014) 1443 [[1310.7439](#)].
- [59] G. Bevilacqua, “unpublished.” 2019.
- [60] A. Denner, S. Dittmaier, S. Kallweit and S. Pozzorini, *NLO QCD corrections to off-shell top-antitop production with leptonic decays at hadron colliders*, *JHEP* **10** (2012) 110 [[1207.5018](#)].
- [61] J. Butterworth et al., *PDF4LHC recommendations for LHC Run II*, *J. Phys. G* **43** (2016) 023001 [[1510.03865](#)].
- [62] S. Bailey, T. Cridge, L.A. Harland-Lang, A.D. Martin and R.S. Thorne, *Parton distributions from LHC, HERA, Tevatron and fixed target data: MSHT20 PDFs*, *Eur. Phys. J. C* **81** (2021) 341 [[2012.04684](#)].
- [63] NNPDF collaboration, *Parton distributions from high-precision collider data*, *Eur. Phys. J. C* **77** (2017) 663 [[1706.00428](#)].
- [64] T.-J. Hou et al., *New CTEQ global analysis of quantum chromodynamics with high-precision data from the LHC*, *Phys. Rev. D* **103** (2021) 014013 [[1912.10053](#)].
- [65] S. Dulat, T.-J. Hou, J. Gao, M. Guzzi, J. Huston, P. Nadolsky et al., *New parton distribution functions from a global analysis of quantum chromodynamics*, *Phys. Rev. D* **93** (2016) 033006 [[1506.07443](#)].
- [66] A. Buckley, J. Ferrando, S. Lloyd, K. Nordström, B. Page, M. Rüfenacht et al., *LHAPDF6: parton density access in the LHC precision era*, *Eur. Phys. J. C* **75** (2015) 132 [[1412.7420](#)].
- [67] M. Cacciari, G.P. Salam and G. Soyez, *The anti- k_t jet clustering algorithm*, *JHEP* **04** (2008) 063 [[0802.1189](#)].
- [68] K. Melnikov, M. Schulze and A. Scharf, *QCD corrections to top quark pair production in association with a photon at hadron colliders*, *Phys. Rev. D* **83** (2011) 074013 [[1102.1967](#)].
- [69] D. Stremmer and M. Worek, *Associated production of a top-quark pair with two isolated photons at the LHC through NLO in QCD*, *JHEP* **08** (2023) 179 [[2306.16968](#)].